Atmos. Chem. Phys., 23, 2747–2764, 2023
https://doi.org/10.5194/acp-23-2747-2023

Atmospheric Chemistry and Physics
Open Access
EGU

Intensive aerosol properties of boreal and regional biomass burning aerosol at Mt. Bachelor Observatory: larger and black carbon (BC)-dominant particles transported from Siberian wildfires

Nathaniel W. May[1], Noah Bernays[1], Ryan Farley[2], Qi Zhang[2], and Daniel A. Jaffe[1]

[1]School of Science, Technology, Engineering, and Mathematics, University of Washington, Bothell, WA 98011, USA
[2]Department of Environmental Toxicology, University of California, Davis, CA 95616, USA

Correspondence: Daniel A. Jaffe (djaffe@uw.edu)

Received: 1 March 2022 – Discussion started: 11 April 2022
Revised: 1 February 2023 – Accepted: 5 February 2023 – Published: 28 February 2023

Abstract. We characterize the aerosol physical and optical properties of 13 transported biomass burning (BB) events. BB events included long-range influence from fires in Alaskan and Siberian boreal forests transported to Mt. Bachelor Observatory (MBO) in the free troposphere (FT) over 8–14+ d and regional wildfires in northern California and southwestern Oregon transported to MBO in the boundary layer (BL) over 10 h to 3 d. Intensive aerosol optical properties and normalized enhancement ratios for BB events were derived from measured aerosol light scattering coefficients (σ_{scat}), aerosol light-absorbing coefficients (σ_{abs}), fine particulate matter (PM_1), and carbon monoxide (CO) measurements made from July to September 2019, with particle size distribution collected from August to September. The observations showed that the Siberian BB events had a lower scattering Ångström exponent (SAE), a higher mass scattering efficiency (MSE; $\Delta\sigma_{scat}/\Delta PM_1$), and a bimodal aerosol size distribution with a higher geometric mean diameter (D_g). We hypothesize that the larger particles and associated scattering properties were due to the transport of fine dust alongside smoke in addition to contributions from condensation of secondary aerosol, coagulation of smaller particles, and aqueous-phase processing during transport. Alaskan and Siberian boreal forest BB plumes were transported long distances in the FT and characterized by lower absorption Ångström exponent (AAE) values indicative of black carbon (BC) dominance in the radiative budget. Significantly elevated AAE values were only observed for BB events with < 1 d transport, which suggests strong production of brown carbon (BrC) in these plumes but limited radiative forcing impacts outside of the immediate region.

1 Introduction

Biomass burning (BB) is a major source of atmospheric aerosols (Bond et al., 2013; Andreae and Merlet, 2001) and significantly impacts public health and regional air quality up to thousands of kilometers from the source (Jaffe et al., 2020; Boucher et al., 2013). BB aerosols also impact global climate by scattering or absorbing solar radiation, acting as cloud condensation nuclei, and altering cloud albedo (Boucher et al., 2013; Spracklen et al., 2011; Pierce et al., 2007). However, there are large uncertainties in BB aerosol formation, evolution, and radiative properties that limit our understanding of their climate impacts (Bond et al., 2013; Boucher et al., 2013, 2020; Bellouin et al., 2020). BB emissions and their associated impacts are likely to increase globally due to hot and dry conditions resulting from climate change, particularly in the western USA (Westerling, 2016; Liu et al., 2014) and sub-Arctic boreal forests of North America and Russia (Flannigan et al., 2009; Stocks et al., 1998).

BB particles are predominantly organic carbon (OC) and black carbon (BC), with some inorganic material (Vakkari et al., 2014; Reid et al., 2005; Zhou et al., 2017). BC is the most significant contributor to the absorption properties of BB particles (Healy et al., 2015; Bond et al., 2013), but OC also contributes to BB particle absorption in the form of brown carbon (BrC) (Andreae and Gelencsér, 2006). BC absorbs nearly uniformly in the range of 0.4 to 1 µm, resulting in an absorption Ångström exponent (AAE) of ∼ 1. High levels of BrC in BB increase AAE values due to its preferential absorption at lower wavelengths of sunlight (Andreae and Gelencsér, 2006). Atmospheric BrC is produced by incomplete combustion (Kirchstetter and Thatcher, 2012; Desyaterik et al., 2013; Lack and Langridge, 2013; Mohr et al., 2013) and secondary formation (Li et al., 2020; Nguyen et al., 2013; Updyke et al., 2012; Laskin et al., 2015). Saleh (2020) describes four classes of brown carbon, with widely varying optical properties, and points out that the BrC properties may depend on the measurement method. Photobleaching reduces the absorption of BrC and therefore significantly impacts the global radiation budget, but there are large uncertainties in this process (Liu et al., 2020a). In contrast, atmospheric BC is chemically inert and primarily produced from flaming combustion (Healy et al., 2015; Bond et al., 2013). In situ aerosol optical measurements are essential to improved modeling of the contributions of BrC and BC-to-BB aerosol absorption properties (Brown et al., 2021).

As plumes age, BB particles grow from their initial diameter (30–100 nm) (Hosseini et al., 2010; Levin et al., 2010) and undergo chemical and physical changes (Carrico et al., 2016; Reid et al., 2005; Vakkari et al., 2014). Changes in particle size are primarily the result of coagulation and the condensation of secondary organic aerosol (SOA) onto existing particles (Reid et al., 2005). However, the condensation of SOA is counterbalanced by loss due to evaporation and oxidation of primary organic aerosol during plume dilution (Collier et al., 2016; Zhou et al., 2017; Garofalo et al., 2019; May et al., 2013). The net condensation/evaporation effect in BB plumes can lead to an increase in PM mass relative to CO due to SOA production (Hobbs et al., 2003; Yokelson et al., 2009; Vakkari et al., 2014), while others have observed limited or no net mass increase (Akagi et al., 2012; Jolleys et al., 2015; Garofalo et al., 2019). Even when normalized PM mass concentrations do not change with age, particle diameter can shift through coagulation and particle–vapor mass transfer (Kleinman et al., 2020). Mie theory predicts that mass scattering efficiency (MSE; σ_{scat}/PM) will increase as the average particle diameter grows toward the measurement wavelength (e.g., 300–700 nm) (Seinfeld and Pandis, 2006). Therefore, understanding the balance of aerosol condensation, evaporation, and removal processes is critical to understanding the scattering properties of aged BB particles.

Airborne mineral dust particles, which can be uplifted into the free troposphere alongside smoke by intense fire-related winds (Wagner et al., 2018), may also impact the radiative forcing of BB emissions. Dust particles are typically larger in size than smoke particles and can produce a net positive or negative radiative forcing depending on surface properties, particle size distribution, and composition (Balkanski et al., 2007; Durant et al., 2009; Russell et al., 2002). However, the climate properties of dust mixed with smoke are so far poorly understood. Dust emissions from fires are most frequently observed in arid regions (Chalbot et al., 2013; Nisantzi et al., 2014; Li et al., 2021) and can be transported over thousands of kilometers (Ansmann et al., 2009; Clements et al., 2008; Baars et al., 2011). Recent observations of lofted dust from fires in the coniferous forests of the western USA (Maudlin et al., 2015; Schlosser et al., 2017; Creamean et al., 2016) and Russia (Popovicheva et al., 2014) suggest that fires in non-arid regions may also emit dust. Despite in situ evidence, fires are not considered to be a source of airborne mineral dust in climate or aerosol models.

In this study, we describe an overview of the intensive optical properties and normalized enhancement ratios of submicron aerosols (PM_1) observed during the summer of 2019 at Mt. Bachelor Observatory (MBO), a remote, high-altitude site in the Pacific Northwest USA. Thirteen BB events were observed, including smoke from nine regional fires (northern California and Oregon, transported < 1–3 d) and four boreal forest fires (Alaska and Siberia, transported 8–10+ d). Aerosol optical and physical properties of these events were explored with respect to source location, emission characteristics, and transport time. The goals of this work are to elucidate how source and transport characteristics of BB events influence their climate impact through aerosol size distributions and the associated scattering properties as well as contributions of BrC and BC to absorption properties.

2 Methods

2.1 Sampling site

Measurements were conducted at MBO, located near the summit of Mt. Bachelor (43.981° N, 121.691° W; 2764 m a.s.l.), from 1 July to 10 September 2019. These observations were part of the larger Fire Influence on Regional to Global Environments and Air Quality (FIREX-AQ) experiment (Liao et al., 2021; Xu et al., 2021; Decker et al., 2021; Wiggins et al., 2021; Makar et al., 2021), which included extensive observations at MBO (Farley et al., 2022). Due to its remote location and limited anthropogenic influence, MBO is an ideal site for measurements of wildfire plumes ranging from locally emitted to long-range transport events (Laing et al., 2016; Baylon et al., 2017; Wigder et al., 2013). The atmospheric conditions during this study were typical for a clean background location as the PM_1 concentrations were relatively low (avg. $\pm 1\sigma$) ($2.8 \pm 3.8\,\mu g\,m^{-3}$), consistent with periods without wildfire influence observed at MBO in 2013 ($.8 \pm 2.8\,\mu g\,sm^{-3}$) (Zhou et al., 2019).

Boundary-layer (BL) dynamics play an important role in the diurnal variation of aerosol composition at MBO. During daytime, upslope flow can mix in BL air to the sampling site, while at night the site is influenced by free troposphere (FT) air masses. These regimes can be differentiated based on ambient water vapor (WV) concentrations. ΔWV is calculated as the difference between the WV ($g\,kg^{-1}$) at the time CO peaked during the event and the WV previously found to demarcate the BL and FT (July–August: $5.23\,g\,kg^{-1}$, September: $4.60\,g\,kg^{-1}$) (Wigder et al., 2013; Baylon et al., 2015; Zhang and Jaffe, 2017). Typically, local smoke plumes will be seen in upslope BL air with a positive ΔWV, whereas distant smoke (Alaska, Siberia) will be transported in the FT with a negative ΔWV.

2.2 CO, aerosol, and meteorology

Details of the CO, aerosol, and meteorology measurements at MBO employed in the current study have been previously described in detail (Laing et al., 2016, 2020; Baylon et al., 2017) and are thus only briefly described here. Basic meteorology measurements include temperature, humidity, and wind speed (Ambrose et al., 2011). CO measurements were made using a Picarro G2302 cavity ring-down spectrometer. Calibrations were performed every 8 h using three different National Oceanographic and Atmospheric Administration (NOAA) calibration gas standards, which are referenced to the World Meteorological Organization (WMO) mole fraction calibration scale (Gratz et al., 2015). Total CO uncertainty based on the precision of calibrations over the campaign was 3 %.

Dry (relative humidity – RH – less than 35 %) aerosol scattering and absorption coefficients, aerosol number size distribution (30–600 nm), and particle mass were measured during the 2019 summer campaign in 5 min averages. An inline 1 µm impactor was located upline of the aerosol instruments. All particle measurements were corrected to standard temperature and pressure (STP; $T = 273.15\,K$, $P = 101.325\,kPa$) and are reported this way throughout the paper. Aerosol light-scattering coefficients (σ_{scat}) were measured by an integrating nephelometer (model 3563, TSI Inc., Shoreview, MN) at 450 nm (blue), 550 nm (green), and 700 nm (red). Data reduction and uncertainty analysis for the scattering data are outlined by Anderson and Ogren (1998).

We measured aerosol light-absorbing coefficients (σ_{abs}) with a 3λ tricolor absorption photometer (TAP, Brechtel Inc., Hayward, CA) at wavelengths 467 nm (blue), 528 nm (green), and 660 nm (red) (Laing et al., 2020). Unless otherwise stated, σ_{scat} and σ_{abs} values represent measurements taken at 550 and 528 nm, respectively. The absorption coefficients were corrected using the filter-loading and aerosol-scattering correction factors derived by Virkkula (2010). Uncertainty calculations were based on those used in a previous study at MBO for measurements with a 3λ Particle Soot Absorption Photometer (PSAP) (Fischer et al., 2010). Combining sources of uncertainties (Anderson et al., 1999; Bond et al., 1999; Virkkula et al., 2005) yielded total uncertainties for σ_{abs} of 30 %–40 % during BB events. Combined scattering uncertainties yielded lower total uncertainties for σ_{scat} of 15 %–20 % during BB events. However, the relative uncertainties between events for absorption and scattering are much lower (< 10 %). This was estimated by calculating the relative standard deviation of the absorption and scattering measurements over a 60 min time window with no wildfire influence at MBO.

The power-law relationship between scattering and wavelength was used to adjust the 550 nm σ_{scat} measurement to 528 nm using Eq. (1) (Laing et al., 2016):

$$\sigma_{scat}^{528} = \sigma_{scat}^{550} \cdot \left(\frac{\lambda_{550}}{\lambda_{528}}\right)^{SAE_{(450,550)}}, \quad (1)$$

where λ is the wavelength and SAE is the scattering Ångström exponent calculated with the 450–550 nm pair. Absorption Ångström exponent (AAE) values were calculated for the σ_{abs} pair of 467 and 660 nm using Eq. (2):

$$AAE = -\frac{\log\left(\frac{\sigma_{abs}^{467}}{\sigma_{abs}^{660}}\right)}{\log\left(\frac{467}{660}\right)}. \quad (2)$$

Uncertainties for the intensive aerosol optical properties SAE and AAE values (Table S1 in the Supplement) were calculated by propagating the uncertainties from the measurements used in the respective calculations using addition in quadrature (Fischer et al., 2010).

We measured the 5 min-averaged dry aerosol number size distribution with a TSI 3938 Scanning Mobility Particle Sizer (SMPS). The SMPS system consisted of a TSI 3082 electrostatic classifier with a TSI 3081 differential mobility analyzer (DMA) and a TSI 3787 water-based condensation particle counter. Geometric mean diameter (D_g) was calculated from lognormal fits of event-averaged size distributions performed with the standard fitting algorithm of Igor Pro analysis software (fit parameters: $x_0 = D_g$, $\text{width} = 2.303 \cdot 2\log\sigma_g$, $A = 2.303 \cdot N/(\pi \cdot \text{width})$).

Dry particle mass under 1 µm (PM_1) was measured with an optical particle counter (OPC, model 1.109, Grimm Technologies, Douglasville, GA). The OPC measures the particle size distribution for particles with aerodynamic diameters from 0.25 to 32 µm in 31 size bins. We note that this size ranges misses a significant fraction of particle mass for smaller particles. For the biomass burning plumes observed in this study, approximately 42 % of the PM_1 mass is accounted for by particles with diameters < 250 µm as determined by the SMPS data. The OPC $PM_{2.5}$ mass concentrations are determined via the manufacturer calibration against standard filter methods (Grimm and Eatough, 2009). The OPC is a USA EPA Federal Equivalent Method for measuring $PM_{2.5}$ mass concentrations. August and September OPC

data were determined to be artificially biased high, which coincided with the installation of a thermodenuder in the aerosol sampling line on 31 July 2019. During this time, the OPC mass concentrations were adjusted to match the SMPS mass concentrations.

2.3 Enhancement ratio calculation

As in prior studies of BB events at MBO (Laing et al., 2016; Briggs et al., 2016), normalized enhancement ratios ($\Delta Y/\Delta X$, NERs) of $\Delta\sigma_{scat}/\Delta CO$, $\Delta\sigma_{abs}/\Delta CO$, and $\Delta PM_1/\Delta CO$ were calculated from the slope of the reduced major axis (RMA) regression of Y plotted against X. Intensive aerosol optical properties mass scattering and mass absorption efficiencies (MSEs and MAEs) were calculated as the NERs of $\Delta\sigma_{scat}/\Delta PM_1$ and $\Delta\sigma_{abs}/\Delta PM_1$, respectively, at 550 nm for σ_{scat} and 528 nm for σ_{abs}. Single scattering albedo (ω) was calculated as the RMA regression of scattering and total extinction (scattering + absorption) using values at 528 nm. In all cases the enhancements are large compared to the background, thus avoiding the problems described by Briggs et al. (2016) for small enhancements above the background. As in prior studies (Laing et al., 2016), uncertainties for the NER calculations were determined from the uncertainties in the extensive properties used in calculating the NERs and the uncertainty of the RMA regression using addition in quadrature.

Precision uncertainty and total uncertainty were calculated as described by Anderson et al. (1999) for all values derived from optical measurements (Table S1). Precision uncertainty is the uncertainty associated with noise and instrument drift. Total uncertainty includes precision uncertainty, the uncertainty associated with the corrections we applied to the data, and the uncertainty associated with the calibration method. Precision uncertainty is best used to compare the individual BB events seen at MBO in this study, whereas total uncertainty is more appropriate to consider when comparing the measurements presented in this study with data collected using other measurement methods.

3 Results and discussion

3.1 BB event identification

The summer of 2019 was a relatively low-activity fire season in the Pacific Northwest, while higher temperatures in the Arctic and sub-Arctic contributed to extensive wildfires across boreal forests in Alaska and Siberia. We identified 13 BB events from July to September 2019, which ranged from 2 to 44 h in duration (Fig. 1). These were split when discernable plumes were separated by a multi-hour drop below the BB event criteria of $\sigma_{scat} > 20\,Mm^{-1}$ and CO > 110 ppbv. BB event criteria was chosen based on our previous work (Wigder et al., 2013). Only 8 % of the 1 h averages at MBO met our criteria for a BB event. Most observed BB events exhibited average σ_{scat} and CO in the ranges of 20–40 Mm^{-1} and 130–170 ppbv, respectively. For comparison, 51 % of the 5 min averages met a higher BB event criterion ($\sigma_{scat} > 20\,Mm^{-1}$ and CO > 150 ppbv) during the high fire year of 2015, where most event average σ_{scat} and CO ranged from 100 to 300 Mm^{-1} and from 200 to 400 ppbv, respectively (Laing et al., 2016). Continuing the approach from Laing et al. (2016), we use the term "event", not "plume", because of the long duration of some of the events and the fact that some BB events observed in 2019 were influenced by emissions from multiple fires. A comparison of CO, σ_{scat}, σ_{abs}, and PM_1 for the BB event and background periods is presented in Fig. S1 in the Supplement.

3.2 Source and transport of BB events

NOAA HYSPLIT air-mass back trajectories and NASA MODIS Aqua and Terra images of smoke were used to identify the origin of each event and estimate the transport time. Two BB events (5–6 July), arriving at MBO with a negative ΔWV (-1.53 $g\,k^{-1}$) (Table 1) indicative of FT transport, were determined to originate from a complex of lightning-initiated fires in boreal forests of the interior of Alaska (AK). The fires started from 22 June to 2 July, and the smoke was transported to MBO over the course of 8–10 d (Fig. S2). Results from a FIREX-AQ model study by Makar et al. (2021) previously suggested wildfires in AK impacted aerosol optical depth (AOD) in North America during this period.

Three BB events with the shortest transport time to MBO observed in this study (∼ 10–15 h) (Fig. S3) originated from the Milepost 97 fire southeast of MBO near Canyonville, OR, which was initiated on 24 July and burned 5300 ha or $5.3 \times 10^7\,m^2$. Of the southwestern Oregon (SW OR) events, two exhibited a positive ΔWV (0.15, 1.47 $g\,k^{-1}$) indicative of BL transport typically observed for local fires and one exhibited a negative ΔWV ($-0.70\,g\,k^{-1}$) indicative of FT arrival (Table 1). Six BB events that had multiple fires active along the back trajectory were categorized as "Regional" in Table 1. The August regional events may have been influenced by emissions from forest fires in Washington, Oregon, and/or California, with transport times estimated to be 1–3 d (Figs. S4 and S5). One August regional event had a ΔWV near zero, indicative of mixed BL and FT influence. The September regional BB events originated from multiple forest fires directly south of MBO in Oregon and California, with transport times estimated to be < 12–48 h (Fig. S6). September regional events were characterized by a positive ΔWV (0.85–4.2 $g\,k^{-1}$) consistent with prior observations of BL transport of regional BB events to MBO (Wigder et al., 2013).

Fires in the boreal forest of Siberia near Lake Baikal were initiated by lightning in July 2019 and continued through August, burning over 3 million ha with smoke transported eastward towards Alaska and the continental USA. Ten-day air-mass back trajectories from MBO for the peak 12 and

Table 1. Overview of intensive plume properties observed in June–September 2019 at MBO. ΔWV was calculated as the difference between the WV at the peak CO of the event and the cutoff value. AAE and SAE values are event averages of hourly data, and all other NERs were calculated as the slope of reduced major axis (RMA) regression of hourly data. MSE is the NER of $\Delta\sigma_{scat}/\Delta PM_1$, and MAE is the NER of $\Delta\sigma_{abs}/\Delta PM_1$. All were calculated from 550 nm (green) measurement wavelength data. Geometric diameter (D_g) was calculated from lognormal fits of event-averaged SMPS size distributions. Category values at the bottom of the table are averages. Events with measurements reported by Farley at al. (2022) are identified by an asterisk.

No.	Event date and time (UTC)	Transport time (days)	Source fire	ΔWV ($g\,kg^{-1}$)	$\Delta\sigma_{scat}/\Delta CO$ ($Mm^{-1}\,ppbv^{-1}$)	$\Delta\sigma_{abs}/\Delta CO$ ($Mm^{-1}\,ppbv^{-1}$)	$\Delta PM_1/\Delta CO$ ($\mu g\,m^{-3}\,ppbv^{-1}$)	MSE ($m^2\,g^{-1}$)	MAE ($m^2\,g^{-1}$)	AAE	SAE	ω	D_g (nm)
1	5 Jul 2019 20:00–6 Jul 2019 07:00	8–10	Alaska	−2.32	0.91	0.07	0.26	3.58	0.28	1.25	1.61	0.93	–
2	7 Jul 2019 02:00–7 Jul 2019 05:00	8–10	Alaska	−0.73	0.96	0.07	0.24	3.98	0.29	1.29	1.79	0.94	–
3	26 Jul 2019 10:00–27 Jul 2019 06:00	< 1	SW OR	0.15	0.88	0.09	0.23	3.82	0.40	2.40	1.95	0.91	–
4	30 Jul 2019 00:00–30 Jul 2019 03:00	< 1	SW OR	−0.70	0.51	0.02	0.19	2.71	0.11	1.48	2.12	0.97	–
5	1 Aug 2019 00:00–2 Aug 2019 11:00	< 1	SW OR*	1.47	0.40	0.03	0.15	2.74	0.22	1.77	2.09	0.93	156
6	5 Aug 2019 23:00–7 Aug 2019 19:00	1–3	Regional	1.17	0.33	0.04	0.11	2.90	0.36	1.28	1.91	0.90	151
7	7 Aug 2019 22:00–8 Aug 2019 01:00	1–3	Regional	6.27	0.35	0.04	0.09	3.72	0.43	0.87	1.99	0.90	156
8	8 Aug 2019 06:00–8 Aug 2019 20:00	1–3	Regional	−2.87	0.37	0.05	0.12	3.19	0.42	1.29	1.98	0.89	158
9	12 Aug 2019 09:00–12 Aug 2019 11:00	> 14	Siberia	−1.43	0.61	0.04	0.12	5.31	0.34	1.36	1.26	0.94	48, 231
10	16 Aug 2019 22:00–17 Aug 2019 13:00	> 14	Siberia*	−2.82	0.33	0.02	0.05	6.63	0.46	1.21	1.49	0.94	92, 278
11	28 Aug 2019 13:00–28 Aug 2019 16:00	1–2	Regional*	0.85	0.46	0.06	0.13	3.50	0.49	1.48	2.17	0.91	151
12	29 Aug 2019 21:00–29 Aug 2019 22:00	1–2	Regional*	4.20	0.42	0.06	0.12	3.47	0.47	1.55	2.31	0.89	147
13	7 Sep 2019 10:00–8 Sep 2019 03:00	< 1–2	Regional*	1.27	0.50	0.07	0.19	2.66	0.38	1.72	2.27	0.90	162
	Alaska ($n = 2$)			−1.52	0.93	0.07	0.25	3.78	0.29	1.27	1.70	0.93	–
	SW OR ($n = 3$)			0.31	0.59	0.05	0.19	3.09	0.24	1.88	2.05	0.94	156
	Siberia ($n = 2$)			−2.82	0.47	0.03	0.08	5.97	0.40	1.29	1.38	0.94	70, 254
	Regional ($n = 6$)			1.27	0.41	0.05	0.13	3.24	0.43	1.36	2.11	0.90	154

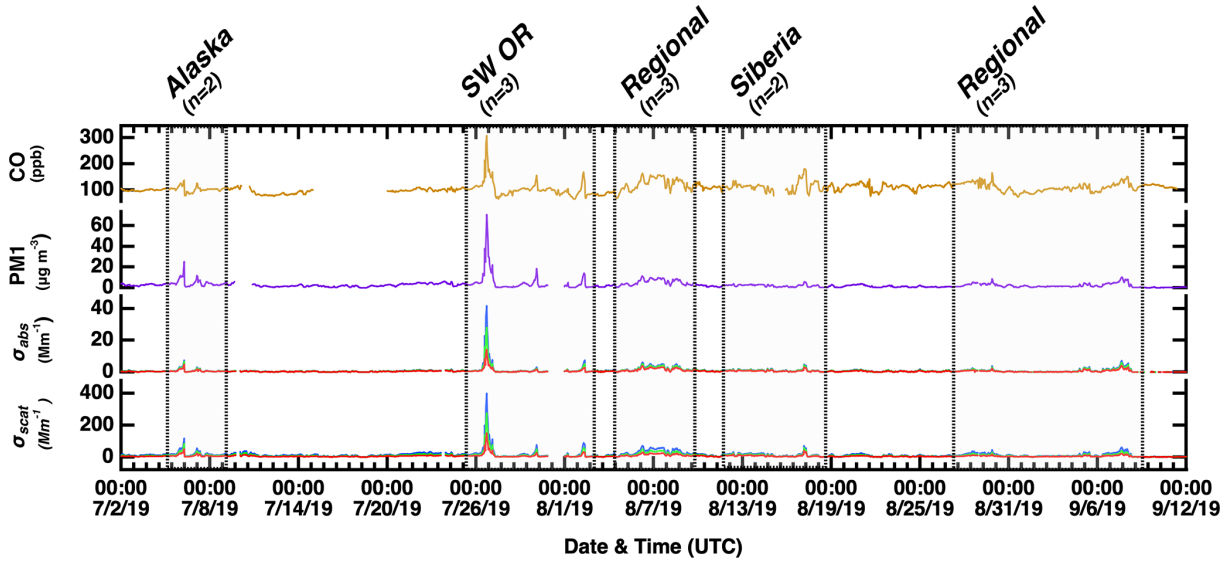

Figure 1. Time series (UTC) of the extensive properties CO (ppb), PM_1 ($\mu g\,m^{-3}$), scattering (Mm^{-1}), and absorption (Mm^{-1}) measured at MBO from 1 July to 14 September 2019. BB event periods are highlighted by grey-filled dashed boxes, with source identification and the number of discrete BB events with $\sigma_{scat,green} > 20\,Mm^{-1}$ and CO > 110 ppbv per period above. The blue, green and red lines in the σ_{abs} and σ_{scat} plots represent measurements in the blue, green and red channels, respectively.

17 August BB events passed over Alaska, but wildfire activity in Alaska had largely subsided. Coinciding measurements by Johnson et al. (2021) observed long-range transported Siberian BB emissions impacting western Canada, with significant aerosol layers between 3 and 10 km a.g.l. measured by lidar on 7, 10, and 13–14 August. Their analysis of MODIS observations and near-real-time satellite-based emissions from the Quick-Fire Emission Database demonstrated enhanced Siberian BB emissions between 19 July and 14 August 2019. In addition, NASA GEOS-CF global model simulations showed that the emissions from the 2019 Siberian fires were transported across the Pacific Ocean and Arctic regions (Johnson et al., 2021). Therefore, Siberian boreal forest fires were determined to be the origin of the 12 and 17 August BB events, with the transport time estimated to be > 14 d (Fig. S7). The negative ΔWV of the Siberian events (-1.43, $-2.82\,g\,k^{-1}$) was indicative of long-range transport to MBO occurring in the FT, which is consistent with established transport pathways of Siberian BB events (Laing et al., 2016).

3.3 Overview of intensive aerosol properties of BB aerosol at MBO

Table 1 provides an overview of NERs and intensive optical properties of 13 BB events of Siberian, Alaskan, SW OR, and regional origin observed at MBO during the summer of 2019. Observed BB event ranges of $\Delta\sigma_{scat}/\Delta CO$ (0.33 to $0.91\,Mm^{-1}\,ppbv^{-1}$), $\Delta\sigma_{abs}/\Delta CO$ (0.02 to $0.09\,Mm^{-1}\,ppbv^{-1}$), and $\Delta PM_1/\Delta CO$ (0.05 to $0.26\,\mu g\,m^{-3}\,ppbv^{-1}$) were comparable to prior summer measurements of transported BB aerosol (Laing et al., 2016; Baylon et al., 2017; Wigder et al., 2013). The range of BB event ω ($\sigma_{scat}/(\sigma_{scat}+\sigma_{abs})$) observed in summer 2019 (0.88–0.95) was lower, (i.e., more absorbing) than previously observed in summer 2015 at MBO (0.95–0.98). The observed range of event-averaged AAE (0.97 to 2.55) was also lower, indicative of greater BC than previous observations in summer 2015 (2.3 to 4.12). The precision and total uncertainties of intensive parameters derived from extensive measurements are provided for these events in Table S1.

3.4 Intensive aerosol properties of BB aerosol at MBO

We observed substantial differences in the intensive physical and optical aerosol properties of Siberian, Alaskan, SW OR, and regional BB events. The average ($\pm1\sigma$) $\Delta PM_1/\Delta CO$ of SW OR ($0.25\pm0.09\,\mu g\,m^{-3}\,ppbv^{-1}$) events transported < 13 h and regional events ($0.17\pm0.10\,\mu g\,m^{-3}\,ppbv^{-1}$) transported 1–3 d were comparable to the $\Delta PM_1/\Delta CO$ emission factor ratio ($0.16\pm0.11\,\mu g\,m^{-3}\,ppbv^{-1}$) for fresh BB in temperate regions (Wigder et al., 2013; Akagi et al., 2012). Therefore, they can be characterized as relatively balanced in PM production and loss. In contrast, Siberian events were characterized by the lowest average $\Delta PM_1/\Delta CO$ ($0.045\pm0.007\,\mu g\,m^{-3}\,ppbv^{-1}$). This result suggests that net PM_1 loss through deposition, evaporation, and/or cloud processing was greater than secondary aerosol production during > 14 d transport in the FT from Siberia. The concurrent measurement of decreasing $\Delta OA/\Delta CO$ with increased transport time in Farley et al. (2022) demonstrates that net OA loss through evaporation and deposition was greater than

growth through secondary processing. Thus, the trend of $\Delta PM_1/\Delta CO$ follows the $\Delta OA/\Delta CO$, which can support the observation of PM_1 loss in this study as OA is the dominant component of PM_1. Wigder et al. (2013) and Weiss-Penzias et al. (2006) previously reported a similar association of decreased $\Delta PM_1/\Delta CO$ with increased transport > 750 km for wildfire smoke arriving at MBO in 2004–2011. However, measurements of elevated $\Delta PM_1/\Delta CO$ for the 8–10 d transported Alaska BB events (0.30 ± 0.07 µg m^{-3} ppbv^{-1}) demonstrate that long-range transport in the FT is not always associated with greater PM_1 loss. Similarly, there was no significant difference in the $\Delta PM_1/\Delta CO$ of summer 2015 Siberian and regional BB events, which Laing et al. (2016) attributed to dry FT transport with limited precipitation. Observations at MBO thus indicate that long-range transport in the FT can yield a wide range of $\Delta PM_1/\Delta CO$ for BB events depending on removal characteristics.

BB aerosols lofted to the FT are typically less likely to be removed by dry deposition and can have a longer atmospheric lifetime of up to 40 d, but wet deposition can enhance removal and therefore reduce lifetime (Bond et al., 2013). Analysis of the impact of wet deposition of Canadian BB plumes demonstrates that it is the dominant mechanism for BC removal from the atmosphere and consequently determines lifetime and atmospheric burden (Franklin et al., 2014; Taylor et al., 2014). Notably, the 2019 Siberian events were transported over the Arctic, where inefficient long-range transport in the summer is attributed to meteorological conditions enhancing wet deposition (Mori et al., 2020). Raut et al. (2017) determined that a large fraction of BC particles in Siberian plumes transported to the Arctic region is mixed with sufficient water-soluble compounds to become CCN-active and is scavenged by large-scale precipitation and wet convective updrafts. They found the role of dry deposition to be minor and limited to the lower troposphere. We used precipitation rates from NOAA HYSPLIT ensemble back trajectories for the AK (Fig. S2, 10 d back-trajectory) and Siberian (Fig. S7, 14 d back-trajectory) BB events as a measure of wet deposition during long-range transport. Average precipitation rates for Siberian events (0.0038 mm h^{-1}) were more than double Alaskan events (0.0016 mm h^{-1}) (Fig. S8). Increased wet deposition during trans-Arctic FT transport thus likely contributed to the reduced $\Delta PM_1/\Delta CO$ in Siberian BB events observed at MBO. Indeed, Farley et al. (2022) concluded that the larger accumulation mode (700 nm D_{va}) in the Siberian BB event PM_1 mass size distribution was the result of increased aqueous-phase cloud processing during transport.

Examination of intensive aerosol absorption properties suggests that the Siberian BB aerosols were generally more absorptive and BC-dominant than the other BB events observed. The average MAE of the Siberian BB events (0.40 m^2 g^{-1}) is similar to the regional events (0.43 m^2 g^{-1}) but higher than the AK and SW OR events (0.29 and 0.24 m^2 g^{-1}, respectively). The greater MAEs in Siberian

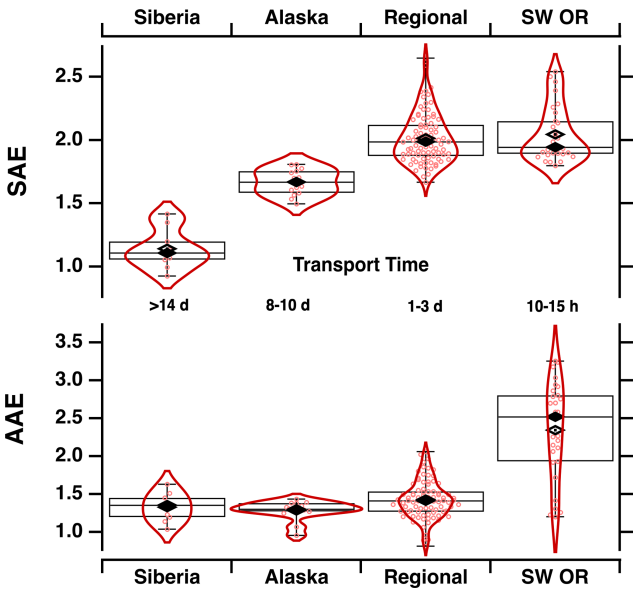

Figure 2. Combined violin and box plots of 1 h average SAE and AAE values for July–September 2019 BB events observed at MBO grouped by source (Siberia, Alaska, regional, SW OR). SAE describes particle sizes, with small values indicating large sizes, and AAE describes particle composition with larger values, indicating greater BrC content. Violin plots in red show the rotated Gaussian kernel probability density, with the mean shown as an open diamond, the median shown as a solid diamond, and 1 h average values shown as open circles. Boxes in black represent upper and lower quartiles, with whiskers representing the minimum and maximum.

events are consistent with higher BC/PM_1 ratios in Siberian events than the other cases identified by Farley et al. (2022) via the concurrent SP-AMS measurements at MBO. Possible reasons for the high mass fractions of BC in Siberian aerosols were wet deposition and enhanced oxidative aging during long-range transport (Farley et al., 2022), which remove BC at a lower rate than the non-BC materials (Liu et al., 2020b). Another possible reason for the higher MAE in Siberian events is greater influence from flaming fires. Indeed, the Siberian events, despite wet deposition and prolonged atmospheric aging, showed higher normalized enhancement ratios of BC ($\Delta BC/\Delta CO$) than the other cases (Farley et al., 2022). Further information on the relative contributions of BC and BrC to BB absorptivity to the transported BB events observed at MBO can be inferred from the intensive aerosol optical property AAE (Figs. 2 and 3). Consistent with SP-AMS measurements, the long-range transported Siberia BB events exhibited low AAE values (1.29) indicative of BC dominance. Alaskan BB events exhibited similar low AAE values (1.27) indicative of BC dominance but were not characterized by enhanced MAE. Prior observations of Siberian events at MBO with similarly enhanced MAE and lower AAE were hypothesized to originate from hotter, more flaming portions of the fires (Laing et al., 2016).

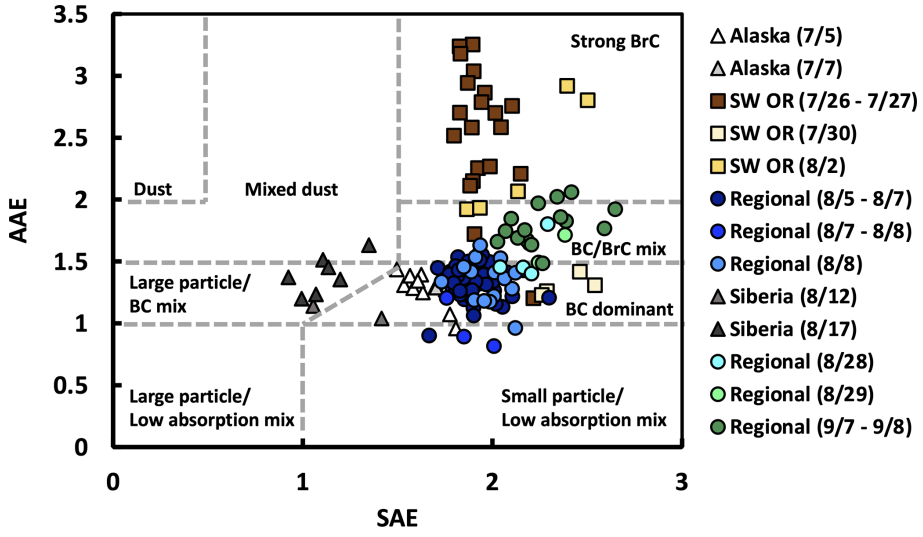

Figure 3. 1 h average SAE and AAE values plotted for all BB events (July–September 2019) observed at MBO, with classification categories from Cappa et al. (2016). SAE describes particle sizes, with small values indicating large sizes, and AAE describes particle composition, with larger values indicating greater BrC content. BB events are colored by the source, with boreal (Alaska, Siberia) shown as triangles in shades of grey, SW OR shown as squares in shades of brown, and regional shown as circles in shades of blue to green.

Flaming fires are characterized by enhanced BC emissions and pyroconvective energy needed to loft the plume high into the atmosphere, where it can undergo long-range transport. ARCTAS-A aircraft measurements in Alaska reported a much larger BC/CO ratio in Siberian fire plumes than North American fire plumes (Kondo et al., 2011), providing further evidence that the emissions from flaming portions comprise the majority of BB transported from Siberian boreal forest fires to North America.

An alternative explanation for low-AAE Siberian and Alaskan BB events is BrC removal by photolysis and oxidation during week-long transport (Laing et al., 2016; Dasari et al., 2019). Analysis of 10 years of aerosol properties at MBO by Zhang and Jaffe (2017) found Asian long-range transport wildfires with lower AAEs (1.45 ± 0.02 and 1.54 ± 0.39) than regional BB events (1.81 ± 0.59). Similarly, we found a general decrease in AAE with increased transport time (Fig. 2). Regional events with 1–3 d transport had a very slightly elevated AAE (mean of 1.36), indicative of slightly more BrC mixed with BC. The highest AAE (mean of 1.88) indicated that stronger BrC was observed for the short-range transported (10–15 h) SW OR events. The highest values of AAE for the SW OR event were associated with the highest PM_1 concentration (Fig. S9), likely due to the presence of nearby, fresh, and concentrated plumes. These results are consistent with the short half life (~ 9 h) of BrC and prior measurements of AAE declining as BrC decays over the course of hours, with little remaining after days of atmospheric transport (Forrister et al., 2015; Hems et al., 2021). A recent laboratory study also found that the imaginary part of BrC could be half decayed in a few hours, in line with the loss of its absorptivity after transport (Liu et al., 2021). Furthermore, the laboratory work by Cappa et al. (2020) and field observations by Wu et al. (2021) suggest that the evolution of AAE and BrC absorptivity with photochemical aging is dependent on the burn conditions and the initial properties of emitted particles. Aerosols from more flaming fires show an initial enhancement of AAE and BrC absorptivity followed by a gradual decrease at longer aging times, while more smoldering aerosols are suggested to experience continuous decrease upon aging. Thus, the highest AAE of the SW OR events could also be related to burning conditions and the initial enhancement of AAE during the short-range transport.

The highest scattering ω (0.94 ± 0.01) was observed in Siberian plumes. The average ω values for the Alaska (0.93 ± 0.01) and SW OR (0.93 ± 0.01) events were elevated compared to the ω for regional events (0.90 ± 0.01). The relatively high ω for Siberian events is thus consistent with our finding of a significantly elevated MSE ($\Delta\sigma_{scat}/\Delta PM_1$) ($8.76 \pm 2.15\ m^2\ g^{-1}$). Satellite observations and 3D atmospheric modeling of 2016 Siberian BB suggested that an observed increase in ω with transport time was likely due to atmospheric processing of SOA, producing an increase in the mass scattering efficiency of BB aerosol (Konovalov et al., 2021). However, the MSE of long-range transported Siberian smoke plumes arriving at MBO in 2015 exhibited no difference from regional events (Laing et al., 2016), and MSE values of aged BB plumes are typically $< 6\ m^2\ g^{-1}$ (Hand and Malm, 2007; McMeeking, 2005). No substantial differences were observed in the average MSE values for AK, SW OR, and regional events (3.65 ± 0.08, 3.40 ± 0.42, $3.97 \pm 0.56\ m^2\ g^{-1}$). According to Mie theory, the uniquely enhanced scattering efficiency of the Siberian BB events sug-

gests an increase in particle size towards the measurement wavelength (Seinfeld and Pandis, 2006).

To better understand the enhanced scattering observed in Siberian events, we related the variation in the MSE values that we observed to aerosol size distributions measured by the SMPS. We found the SMPS geometric mean diameter (D_g) to be correlated with MSE across all 2019 BB events ($R^2 = 0.93$) (Fig. 4), which is consistent with Mie theory and previous ambient observations of aged BB (Lowenthal and Kumar, 2004; Laing et al., 2016) and laboratory studies (McMeeking, 2005). However, MSE in 2019 was $\sim 40\,\%$ higher than 2015 at a similar D_g (Laing et al., 2016). It was suggested that larger size distributions in 2015 BB events may be the result of more concentrated BB plumes with slower particle evaporation rates, leading to greater net PM and SOA accumulation during aging (Hodshire et al., 2019). This conclusion was supported by the correlation of 2015 BB event D_g with CO, σ_{scat}, and PM_1, which can be thought of as surrogates for plume concentration. However, D_g was not found to be correlated with CO, σ_{scat}, or PM_1 in 2019, with the largest particles observed in the more dilute Siberian event. Plume concentration does not appear to be the determining factor in the particle size of 2019 BB events.

SAE is an intensive aerosol optical property that can be used as a measure of particle size, with small values indicating large sizes (Kleinman et al., 2020). All SAE values here (Figs. 2 and 3) are expected to be > 1, because only fine particles (PM_1) were measured. August–September BB event SAEs were negatively correlated with D_g ($R^2 = 0.85$) (Fig. 4), generally supporting its use as a measure of particle size. SW OR and regional events exhibited elevated SAE values characteristic of the smaller size distributions of fresh to moderately aged BB plumes (May et al., 2014; Levin et al., 2010). In contrast, both long-range transported AK and Siberian events exhibited lower SAE values, suggesting that long-range transport may produce a shift in BB aerosol to larger particle sizes (Jung et al., 2012). However, particle morphology, composition, and coatings can also alter SAE values. Thin coatings on BC particles may yield lower SAE values (Zhang et al., 2020).

Multiple field observations have observed D_g and MSE to increase as a function of photochemical age (e.g., Akagi et al., 2012; Carrico et al., 2016; Kleinman et al., 2020). An increase in MSE with age suggests a rearrangement of particle mass that favors large-diameter efficient scatters at the expense of small inefficient scatters. This could be the result of a transfer of mass between the gas and particulate phases (i.e., condensation) and amongst particles (i.e., coagulation) (Kleinman et al., 2020). We explore the relationship between SMPS number size distributions and SP-AMS aerosol composition measurements in Sect. 3.5 to examine the potential influence of aerosol growth processes during transport of Siberian BB events.

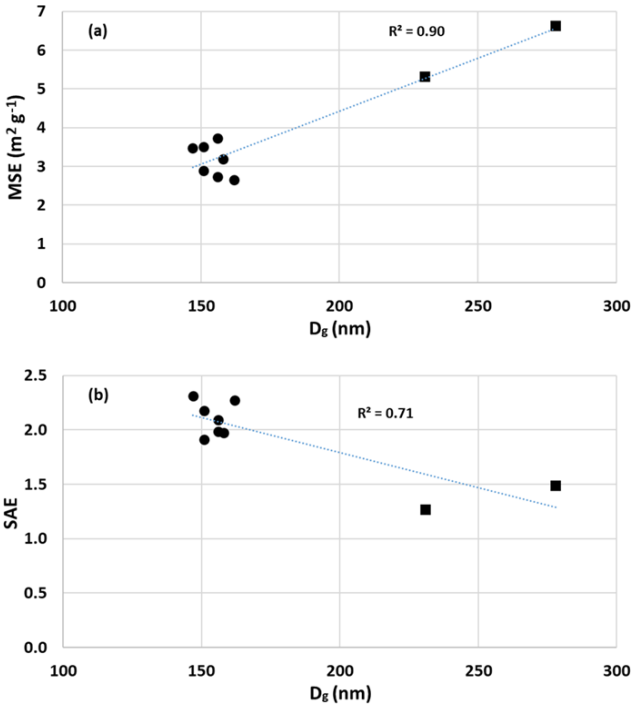

Figure 4. **(a)** Mass scattering efficiency (MSE) versus geometric mean diameter (D_g) from the SMPS size distribution of the 2019 BB events observed at MBO, with linear regression and correlation coefficients shown. **(b)** D_g and SAE for the August–September 2019 events observed at MBO, with linear regression and correlation coefficients shown. The Siberian BB events are shown with squares and all others as circles. Both relationships are statistically significant with $P < 0.05$.

While secondary aerosol growth and/or coagulation during transport present plausible explanations for larger particles, we also consider the unexpected contribution of dust mixed with smoke. SAE was previously used by Zhang and Jaffe (2016) to identify larger particle sizes in long-range transport of industrial pollution from Asia, which was suggested to be due to mixing with mineral dust sources. In addition, prior measurements in spring have identified an association of dust mixed with smoke in long-range transported plumes from Asia with a lower SAE at MBO (Fischer et al., 2010). Elevated AAE alongside low SAE (Fig. 3) can be indicative of dust aerosols with enhanced absorption at short wavelengths (Bergstrom et al., 2007; Titos et al., 2017). However, the distribution and average AAE of the Siberian BB events were similar to the Alaskan BB events.

Wagner et al. (2018) illustrated via high-resolution eddy simulation that the energy released by wildfires leads to a significant increase in near-surface wind speed and enhanced dust uplift potential. Based on this model, we hypothesize that the enhanced pyroconvective energy of Siberian fires that injects BC into the FT (Laing et al., 2016) may also produce intense fire-related winds that lofted fine dust along-

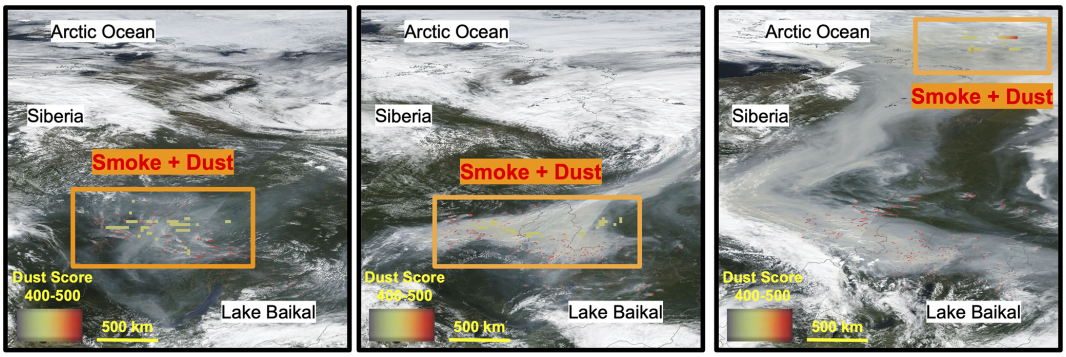

Figure 5. **(a)** 1 August, **(b)** 5 August, and **(c)** 10 August 2019 NASA MODIS true color satellite images of Siberian boreal forest fires. Fire and thermal anomalies shown in red dots and Dust Score values shown in pixels colored according to the embedded scale. Areas of dust score and visible smoke are outlined in orange boxes.

side smoke into the FT, where it was transported to MBO. Enhancements in much larger coarse-mode particles are typically used to identify the influence of dust (Lee and Cho, 2007), but recent measurements in the western USA found evidence of fine-mode dust mixed with smoke (Maudlin et al., 2015; Schlosser et al., 2017; Jahn et al., 2021). Therefore, we propose that dust mixed with smoke may have contributed to the enhanced larger particle size distribution in the Siberian BB events. In the following sections we present satellite data showing the transport of dust alongside smoke from Siberian boreal forest fires (Sect. 3.4) and SMPS size distributions to examine the potential contributions of dust to Siberian BB events (Sect. 3.5).

3.5 Satellite identification of dust mixed with smoke in Siberian BB events

The NASA Dust Score satellite product, which is computed from infrared channels of the NASA Aqua/AIRS satellite (DeSouza-Machado et al., 2010), was overlaid onto MODIS images to examine the presence of dust mixed with smoke emitted and transported from identified source fires. Dust Score is a qualitative representation of the presence of dust in the atmosphere, with values ranging from 400 to 500 here. The sensor resolution is 45 km with once-per-day coverage. A significant Dust Score (> 360) was not observed near the origin of the Alaskan, SW OR and regional BB events. In contrast, a large geographic area of dust mixed and transported with smoke is observed in time series (5, 7, 10 August) of Dust Score overlaid on MODIS images of Siberian boreal forest fires (Fig. 5).

We used V3.30 aerosol classification products from the Cloud-Aerosol Lidar with Orthogonal Polarization (CALIOP) instrument on the Cloud-Aerosol Lidar Infrared Pathfinder Satellite Observation (CALIPSO) satellite (Winker et al., 2010) to further examine long-range transport of dust mixed with smoke for Alaskan and Siberian BB events. A time series (10, 12, and 17 August) of the NASA CALIPSO aerosol-type satellite cross sections suggests that "dust", "polluted dust", and "smoke" underwent transport in the FT from Siberia to the western USA (Fig. S10). A time series (30 June and 2 and 5 July) of the NASA CALIPSO aerosol-type satellite cross sections shows "polluted continental/smoke" and "smoke", with comparatively minor contributions from "dust" transported from AK to the western USA (Fig. S11). CALIPSO has previously been used in a similar manner to identify the transport of dust with smoke in plumes of Asian origin arriving at MBO in spring (Fischer et al., 2009). However, due to the lack of direct measurement of dust in this study, we cannot conclude with confidence that dust was present in the Siberian BB events. Nevertheless, the CALIPSO result suggests that fires in the Siberian boreal forest, as well as other non-arid regions, should be considered a source of airborne mineral dust.

3.6 Aerosol number size distribution and composition

Aerosol number size distribution (30–600 nm) was measured by SMPS for nine BB events as well as interstitial background periods in August and September 2019 (Fig. 6). Geometric diameters (D_g) of aerosol number size distributions are presented in Table 1, with further size distribution parameters detailed in Table S2. The SW OR and regional events exhibited similar unimodal number size distributions, with D_g values between 146 and 162 nm. A prominent "tail" consisting of higher-than-expected number concentrations of small-diameter particles (30–90 nm) was observed in the size distribution for events arriving in the BL at MBO, similar to results in Laing et al. (2016). Background periods exhibited a unimodal number size distribution with a smaller D_g (101 nm). Siberian events were characterized by bimodal number size distributions, with a larger accumulation-mode peak > 200 nm and a lower ultrafine-mode peak < 100 nm

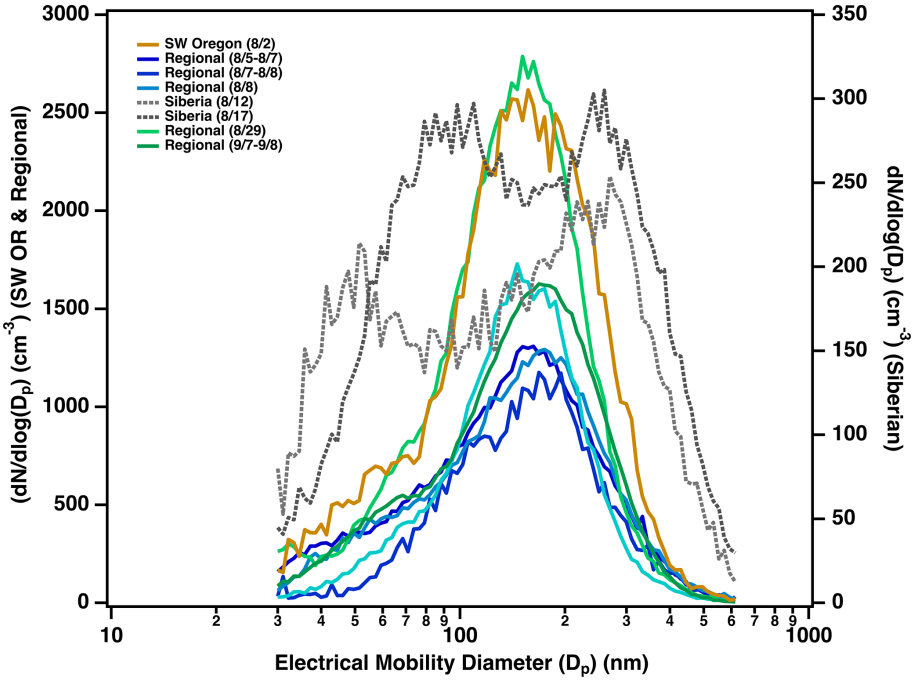

Figure 6. Event-averaged aerosol number size distributions in $\mathrm{d}N/\mathrm{d}\log(D_\mathrm{p})$ measured by SMPS for the SW OR (left axis), regional (left axis), and Siberian (right axis) BB events identified in August–September 2019 at MBO as well as the background average aerosol number size distribution (right axis).

(Fig. 6), which could reflect new particle formation following cloud processing (Taylor et al., 2014).

The larger accumulation modes of Siberian events suggest contributions from fine dust particles identified in the Dust Score and CALIPSO satellite products. Submicron dust particles as small as 300 nm have been observed in Africa (Kaaden et al., 2009; Kandler et al., 2009; Denjean et al., 2016), and Asian dust storms have been found to be correlated with an increase in 200–500 nm particles (Liang et al., 2013). Furthermore, submicron dust particles in the size range measured by SMPS in this study are expected to be transported more efficiently than the coarse dust particles that may have been present in the initial Siberian BB plume. Farley et al. (2022) measured a larger mass-weighted size distribution by SP-AMS for Siberian BB events compared to regional BB events. However, without aerosol chemical composition measurements of dust, which are not measured by SP-AMS, we cannot conclude with confidence that dust was present in the Siberian BB events.

Ultrafine particles are typically not the result of long-range transport, as it would be expected that small particles would grow through coagulation relatively quickly. Therefore, the observed < 100 nm modes in long-range transported Siberian BB events are indicative of the influence of entrained background air and/or new particle formation (NPF). A year-long study at the Swiss mountaintop observatory Jungfraujoch suggested summer NPF to be triggered by previously entrained precursors or by boundary-layer injections on the same day (Tröstl et al., 2016).

4 Conclusions

We characterized the physical and optical properties of 13 aged biomass burning events observed at Mt. Bachelor Observatory in summer 2019. Our conclusions were as follows.

- Low $\Delta\mathrm{PM}_1/\Delta\mathrm{CO}$ values of Siberian BB events are likely the result of enhanced wet deposition in trans-Pacific and trans-Arctic FT transport from Siberia to MBO.

- BB events from Siberian and Alaskan boreal forest fires with multi-day transport in the FT were associated with lower AAE values indicative of BC dominance. The aerosols during these events have lower AAE values compared to regional BB events. We propose two hypotheses for the BC dominance of boreal forest BB events.

  a. The short half life of BrC leads to its decays over the course of hours, with little remaining in the plume after a week or more of transport.

  b. Siberian events with higher MAE originated from hotter, more flaming portions of the fires.

- BB events from a southwestern Oregon wildfire arriving in the BL with a short transport time (< 15 h) were associated with the highest AAE indicative of BrC contributions to absorption.
- The higher D_g, lower SAE, and higher MSE of Siberian BB events reflected contributions from large particles, for which we propose two hypotheses.
    a. Enhanced secondary processing during long-range transport leading to particle growth, which is supported by SP-AMS measurements of enhanced low-volatility organics and sulfate in Siberian BB reported by Farley et al. (2022).
    b. Fine dust transported alongside smoke, which is supported by CALIPSO and Dust Score satellite products of dust mixed with smoke originating from Siberian boreal forest fires.

Data availability. The Mt. Bachelor Observatory 2019 datasets are permanently archived at the University of Washington Research Works site: http://hdl.handle.net/1773/48342 (Jaffe, 2023).

Supplement. The supplement related to this article is available online at: https://doi.org/10.5194/acp-23-2747-2023-supplement.

Author contributions. DJ and NM designed the study, developed the analysis protocols, and wrote the initial manuscript. NB, RF and QZ provided data, provided comments on the analysis, and contributed and reviewed the final manuscript.

Competing interests. The contact author has declared that none of the authors has any competing interests.

Disclaimer. Publisher's note: Copernicus Publications remains neutral with regard to jurisdictional claims in published maps and institutional affiliations.

Acknowledgements. The Mt. Bachelor Observatory is supported by the National Science Foundation (grant no. AGS-1447832) and the National Oceanic and Atmospheric Administration (contract no. RA-133R-16-SE-0758). Ryan Farley and Qi Zhang were financially supported by the National Science Foundation (grant no. AGS-1829803) and the DOE Atmospheric System Research Program (grant no. DESC0022140). The authors are grateful to the NOAA Air Resources Laboratory (ARL) for the provision of the HYSPLIT transport model used in this publication. The CALIPSO satellite products were supplied by the NASA Langley Research Center.

Financial support. This research has been supported by the Division of Atmospheric and Geospace Sciences (grant nos. AGS-1447832 and AGS-1829803) and the National Oceanic and Atmospheric Administration (grant no. RA-133R-16-SE-0758).

Review statement. This paper was edited by Dantong Liu and reviewed by three anonymous referees.

References

Akagi, S. K., Craven, J. S., Taylor, J. W., McMeeking, G. R., Yokelson, R. J., Burling, I. R., Urbanski, S. P., Wold, C. E., Seinfeld, J. H., Coe, H., Alvarado, M. J., and Weise, D. R.: Evolution of trace gases and particles emitted by a chaparral fire in California, Atmos. Chem. Phys., 12, 1397–1421, https://doi.org/10.5194/acp-12-1397-2012, 2012.

Ambrose, J. L., Reidmiller, D. R., and Jaffe, D. A.: Causes of high O_3 in the lower free troposphere over the Pacific Northwest as observed at the Mt. Bachelor Observatory, Atmos. Environ., 45, 5302–5315, https://doi.org/10.1016/j.atmosenv.2011.06.056, 2011.

Anderson, T. L. and Ogren, J. A.: Determining Aerosol Radiative Properties Using the TSI 3563 Integrating Nephelometer, Aerosol Sci. Tech., 29, 57–69, https://doi.org/10.1080/02786829808965551, 1998.

Anderson, T. L., Covert, D. S., Wheeler, J. D., Harris, J. M., Perry, K. D., Trost, B. E., Jaffe, D. J., and Ogren, J. A.: Aerosol backscatter fraction and single scattering albedo: Measured values and uncertainties at a coastal station in the Pacific Northwest, J. Geophys. Res.-Atmos., 104, 26793–26807, https://doi.org/10.1029/1999JD900172, 1999.

Andreae, M. O. and Gelencsér, A.: Black carbon or brown carbon? The nature of light-absorbing carbonaceous aerosols, Atmos. Chem. Phys., 6, 3131–3148, https://doi.org/10.5194/acp-6-3131-2006, 2006.

Andreae, M. O. and Merlet, P.: Emission of trace gases and aerosols from biomass burning, Global Biogeochem. Cy., 15, 955–966, https://doi.org/10.1029/2000GB001382, 2001.

Ansmann, A., Baars, H., Tesche, M., Müller, D., Althausen, D., Engelmann, R., Pauliquevis, T., and Artaxo, P.: Dust and smoke transport from Africa to South America: Lidar profiling over Cape Verde and the Amazon rainforest, Geophys. Res. Lett., 36, L11802, https://doi.org/10.1029/2009GL037923, 2009.

Baars, H., Ansmann, A., Althausen, D., Engelmann, R., Artaxo, P., Pauliquevis, T., and Souza, R.: Further evidence for significant smoke transport from Africa to Amazonia, Geophys. Res. Lett., 38, L20802, https://doi.org/10.1029/2011GL049200, 2011.

Balkanski, Y., Schulz, M., Claquin, T., and Guibert, S.: Reevaluation of Mineral aerosol radiative forcings suggests a better agreement with satellite and AERONET data, Atmos. Chem. Phys., 7, 81–95, https://doi.org/10.5194/acp-7-81-2007, 2007.

Baylon, P., Jaffe, D. A., Wigder, N. L., Gao, H., and Hee, J.: Ozone enhancement in western US wildfire plumes at the Mt. Bachelor Observatory: The role of NO_x, Atmos. Environ., 109, 297–304, https://doi.org/10.1016/j.atmosenv.2014.09.013, 2015.

Baylon, P., Jaffe, D. A., de Gouw, J., and Warneke, C.: Influence of Long-Range Transport of Siberian Biomass Burning at the Mt. Bachelor Observatory during the

Spring of 2015, Aerosol Air Qual. Res., 17, 2751–2761, https://doi.org/10.4209/aaqr.2017.06.0213, 2017.

Bellouin, N., Quaas, J., Gryspeerdt, E., Kinne, S., Stier, P., Watson-Parris, D., Boucher, O., Carslaw, K. S., Christensen, M., Daniau, A.-L., Dufresne, J.-L., Feingold, G., Fiedler, S., Forster, P., Gettelman, A., Haywood, J. M., Lohmann, U., Malavelle, F., Mauritsen, T., McCoy, D. T., Myhre, G., Mülmenstädt, J., Neubauer, D., Possner, A., Rugenstein, M., Sato, Y., Schulz, M., Schwartz, S. E., Sourdeval, O., Storelvmo, T., Toll, V., Winker, D., and Stevens, B.: Bounding Global Aerosol Radiative Forcing of Climate Change, Rev. Geophys., 58, e2019RG000660, https://doi.org/10.1029/2019RG000660, 2020.

Bergstrom, R. W., Pilewskie, P., Russell, P. B., Redemann, J., Bond, T. C., Quinn, P. K., and Sierau, B.: Spectral absorption properties of atmospheric aerosols, Atmos. Chem. Phys., 7, 5937–5943, https://doi.org/10.5194/acp-7-5937-2007, 2007.

Bond, T. C., Anderson, T. L., and Campbell, D.: Calibration and Intercomparison of Filter-Based Measurements of Visible Light Absorption by Aerosols, Aerosol Sci. Tech., 30, 582–600, 1999.

Bond, T. C., Doherty, S. J., Fahey, D. W., Forster, P. M., Berntsen, T., DeAngelo, B. J., Flanner, M. G., Ghan, S., Kärcher, B., Koch, D., Kinne, S., Kondo, Y., Quinn, P. K., Sarofim, M. C., Schultz, M. G., Schulz, M., Venkataraman, C., Zhang, H., Zhang, S., Bellouin, N., Guttikunda, S. K., Hopke, P. K., Jacobson, M. Z., Kaiser, J. W., Klimont, Z., Lohmann, U., Schwarz, J. P., Shindell, D., Storelvmo, T., Warren, S. G., and Zender, C. S.: Bounding the role of black carbon in the climate system: A scientific assessment, J. Geophys. Res.-Atmos., 118, 5380–5552, https://doi.org/10.1002/jgrd.50171, 2013.

Boucher, O., Randall, D., Artaxo, P., Bretherton, C., Feingold, G., Forster, P., Kerminen, V.-M., Kondo, Y., Liao, H., Lohmann, U., Rasch, P., Satheesh, S. K., Sherwood, S., Stevens, B., and Zhang, X. Y.: Clouds and Aerosols, in: Climate Change 2013: The Physical Science Basis, Contribution of Working Group I to the Fifth Assessment Report of the Intergovernmental Panel on Climate Change, edited by: Stocker, T. F., Qin, D., Plattner, G.-K., Tignor, M., Allen, S. K., Boschung, J., Nauels, A., Xia, Y., Bex, V., and Midgley, P. M., Cambridge University Press, Cambridge, UKand New York, NY, USA, 571–658, https://doi.org/10.1017/CBO9781107415324.016, 2013.

Boucher, O., Servonnat, J., Albright, A. L., Aumont, O., Balkanski, Y., Bastrikov, V., Bekki, S., Bonnet, R., Bony, S., Bopp, L., Braconnot, P., Brockmann, P., Cadule, P., Caubel, A., Cheruy, F., Codron, F., Cozic, A., Cugnet, D., D'Andrea, F., Davini, P., Lavergne, C., Denvil, S., Deshayes, J., Devilliers, M., Ducharne, A., Dufresne, J.-L., Dupont, E., Éthé, C., Fairhead, L., Falletti, L., Flavoni, S., Foujols, M.-A., Gardoll, S., Gastineau, G., Ghattas, J., Grandpeix, J.-Y., Guenet, B., Guez, Lionel, E., Guilyardi, E., Guimberteau, M., Hauglustaine, D., Hourdin, F., Idelkadi, A., Joussaume, S., Kageyama, M., Khodri, M., Krinner, G., Lebas, N., Levavasseur, G., Lévy, C., Li, L., Lott, F., Lurton, T., Luyssaert, S., Madec, G., Madeleine, J.-B., Maignan, F., Marchand, M., Marti, O., Mellul, L., Meurdesoif, Y., Mignot, J., Musat, I., Ottlé, C., Peylin, P., Planton, Y., Polcher, J., Rio, C., Rochetin, N., Rousset, C., Sepulchre, P., Sima, A., Swingedouw, D., Thiéblemont, R., Traore, A. K., Vancoppenolle, M., Vial, J., Vialard, J., Viovy, N., and Vuichard, N.: Presentation and Evaluation of the IPSL-CM6A-LR Climate Model, J. Adv. Model. Earth Syst., 12, e2019MS002010, https://doi.org/10.1029/2019MS002010, 2020.

Briggs, N. L., Jaffe, D. A., Gao, H., Hee, J. R., Baylon, P. M., Zhang, Q., Zhou, S., Collier, S. C., Sampson, P. D., and Cary, R. A.: Particulate Matter, Ozone, and Nitrogen Species in Aged Wildfire Plumes Observed at the Mount Bachelor Observatory, Aerosol Air Qual. Res., 16, 3075–3087, https://doi.org/10.4209/aaqr.2016.03.0120, 2016.

Brown, H., Liu, X., Pokhrel, R., Murphy, S., Lu, Z., Saleh, R., Mielonen, T., Kokkola, H., Bergman, T., Myhre, G., Skeie, R. B., Watson-Paris, D., Stier, P., Johnson, B., Bellouin, N., Schulz, M., Vakkari, V., Beukes, J. P., van Zyl, P. G., Liu, S., and Chand, D.: Biomass burning aerosols in most climate models are too absorbing, Nat. Commun., 12, 277, https://doi.org/10.1038/s41467-020-20482-9, 2021.

Cappa, C. D., Kolesar, K. R., Zhang, X., Atkinson, D. B., Pekour, M. S., Zaveri, R. A., Zelenyuk, A., and Zhang, Q.: Understanding the optical properties of ambient sub- and supermicron particulate matter: results from the CARES 2010 field study in northern California, Atmos. Chem. Phys., 16, 6511–6535, https://doi.org/10.5194/acp-16-6511-2016, 2016.

Cappa, C. D., Lim, C. Y., Hagan, D. H., Coggon, M., Koss, A., Sekimoto, K., de Gouw, J., Onasch, T. B., Warneke, C., and Kroll, J. H.: Biomass-burning-derived particles from a wide variety of fuels – Part 2: Effects of photochemical aging on particle optical and chemical properties, Atmos. Chem. Phys., 20, 8511–8532, https://doi.org/10.5194/acp-20-8511-2020, 2020.

Carrico, C. M., Prenni, A. J., Kreidenweis, S. M., Levin, E. J. T., McCluskey, C. S., DeMott, P. J., McMeeking, G. R., Nakao, S., Stockwell, C., and Yokelson, R. J.: Rapidly evolving ultrafine and fine mode biomass smoke physical properties: Comparing laboratory and field results, J. Geophys. Res.-Atmos., 121, 5750–5768, https://doi.org/10.1002/2015JD024389, 2016.

Chalbot, M.-C., McElroy, B., and Kavouras, I. G.: Sources, trends and regional impacts of fine particulate matter in southern Mississippi valley: significance of emissions from sources in the Gulf of Mexico coast, Atmos. Chem. Phys., 13, 3721–3732, https://doi.org/10.5194/acp-13-3721-2013, 2013.

Clements, C. B., Zhong, S., Bian, X., Heilman, W. E., and Byun, D. W.: First observations of turbulence generated by grass fires, J. Geophys. Res.-Atmos., 113, D22102, https://doi.org/10.1029/2008JD010014, 2008.

Collier, S., Zhou, S., Onasch, T. B., Jaffe, D. A., Kleinman, L., Sedlacek, A. J., Briggs, N. L., Hee, J., Fortner, E., Shilling, J. E., Worsnop, D., Yokelson, R. J., Parworth, C., Ge, X., Xu, J., Butterfield, Z., Chand, D., Dubey, M. K., Pekour, M. S., Springston, S., and Zhang, Q.: Regional Influence of Aerosol Emissions from Wildfires Driven by Combustion Efficiency: Insights from the BBOP Campaign, Environ. Sci. Technol., 50, 8613–8622, https://doi.org/10.1021/acs.est.6b01617, 2016.

Creamean, J. M., Neiman, P. J., Coleman, T., Senff, C. J., Kirgis, G., Alvarez, R. J., and Yamamoto, A.: Colorado air quality impacted by long-range-transported aerosol: a set of case studies during the 2015 Pacific Northwest fires, Atmos. Chem. Phys., 16, 12329–12345, https://doi.org/10.5194/acp-16-12329-2016, 2016.

Dasari, S., Andersson, A., Bikkina, S., Holmstrand, H., Budhavant, K., Satheesh, S., Asmi, E., Kesti, J., Backman, J., Salam, A., Bisht, D. S., Tiwari, S., Hameed, Z., and Gustafsson, Ö.: Photochemical degradation affects the light absorption of water-

soluble brown carbon in the South Asian outflow, Sci. Adv., 5, eaau8066, https://doi.org/10.1126/sciadv.aau8066, 2019.

Decker, Z. C. J., Wang, S., Bourgeois, I., Campuzano Jost, P., Coggon, M. M., DiGangi, J. P., Diskin, G. S., Flocke, F. M., Franchin, A., Fredrickson, C. D., Gkatzelis, G. I., Hall, S. R., Halliday, H., Hayden, K., Holmes, C. D., Huey, L. G., Jimenez, J. L., Lee, Y. R., Lindaas, J., Middlebrook, A. M., Montzka, D. D., Neuman, J. A., Nowak, J. B., Pagonis, D., Palm, B. B., Peischl, J., Piel, F., Rickly, P. S., Robinson, M. A., Rollins, A. W., Ryerson, T. B., Sekimoto, K., Thornton, J. A., Tyndall, G. S., Ullmann, K., Veres, P. R., Warneke, C., Washenfelder, R. A., Weinheimer, A. J., Wisthaler, A., Womack, C., and Brown, S. S.: Novel Analysis to Quantify Plume Crosswind Heterogeneity Applied to Biomass Burning Smoke, Environ. Sci. Technol., 55, 15646–15657, https://doi.org/10.1021/acs.est.1c03803, 2021.

Denjean, C., Formenti, P., Desboeufs, K., Chevaillier, S., Triquet, S., Maillé, M., Cazaunau, M., Laurent, B., Mayol-Bracero, O. L., Vallejo, P., Quiñones, M., Gutierrez-Molina, I. E., Cassola, F., Prati, P., Andrews, E., and Ogren, J.: Size distribution and optical properties of African mineral dust after intercontinental transport, J. Geophys. Res.-Atmos., 121, 7117–7138, https://doi.org/10.1002/2016JD024783, 2016.

DeSouza-Machado, S. G., Strow, L. L., Imbiriba, B., McCann, K., Hoff, R. M., Hannon, S. E., Martins, J. v, Tanré, D., Deuzé, J. L., Ducos, F., and Torres, O.: Infrared retrievals of dust using AIRS: Comparisons of optical depths and heights derived for a North African dust storm to other collocated EOS A-Train and surface observations, J. Geophys. Res., 115, D15201, https://doi.org/10.1029/2009JD012842, 2010.

Desyaterik, Y., Sun, Y., Shen, X., Lee, T., Wang, X., Wang, T., and Collett, J. L.: Speciation of "brown" carbon in cloud water impacted by agricultural biomass burning in eastern China, J. Geophys. Res.-Atmos., 118, 7389–7399, https://doi.org/10.1002/jgrd.50561, 2013.

Durant, A. J., Harrison, S. P., Watson, I. M., and Balkanski, Y.: Sensitivity of direct radiative forcing by mineral dust to particle characteristics, Prog. Phys. Geogr., 33, 80–102, https://doi.org/10.1177/0309133309105034, 2009.

Farley, R., Bernays, N., Ketcherside, D., Jaffe, D. A., Hu, L., Zhou, S., Collier, S., and Zhang, Q.: Persistent Influence of Wildfire Emissions in the Western United States and Characteristics of Aged Biomass Burning Organic Aerosols Under Clean Air Conditions, Environ. Sci. Technol., 56, 3645–3657, https://doi.org/10.1021/acs.est.1c07301, 2022.

Fischer, E. V., Hsu, N. C., Jaffe, D. A., Jeong, M.-J., and Gong, S. L.: A decade of dust: Asian dust and springtime aerosol load in the U.S. Pacific Northwest, Geophys. Res. Lett., 36, L03821, https://doi.org/10.1029/2008GL036467, 2009.

Fischer, E. V., Jaffe, D. A., Marley, N. A., Gaffney, J. S., and Marchany-Rivera, A.: Optical properties of aged Asian aerosols observed over the U.S. Pacific Northwest, J. Geophys. Res.-Atmos., 115, D20209, https://doi.org/10.1029/2010JD013943, 2010.

Flannigan, M., Stocks, B., Turetsky, M., and Wotton, M.: Impacts of climate change on fire activity and fire management in the circumboreal forest, Global Change Biol., 15, 549–560, https://doi.org/10.1111/j.1365-2486.2008.01660.x, 2009.

Forrister, H., Liu, J., Scheuer, E., Dibb, J., Ziemba, L., Thornhill, K. L., Anderson, B., Diskin, G., Perring, A. E., Schwarz, J. P., Campuzano-Jost, P., Day, D. A., Palm, B. B., Jimenez, J. L., Nenes, A., and Weber, R. J.: Evolution of brown carbon in wildfire plumes, Geophys. Res. Lett., 42, 4623–4630, https://doi.org/10.1002/2015GL063897, 2015.

Franklin, J. E., Drummond, J. R., Griffin, D., Pierce, J. R., Waugh, D. L., Palmer, P. I., Parrington, M., Lee, J. D., Lewis, A. C., Rickard, A. R., Taylor, J. W., Allan, J. D., Coe, H., Walker, K. A., Chisholm, L., Duck, T. J., Hopper, J. T., Blanchard, Y., Gibson, M. D., Curry, K. R., Sakamoto, K. M., Lesins, G., Dan, L., Kliever, J., and Saha, A.: A case study of aerosol scavenging in a biomass burning plume over eastern Canada during the 2011 BORTAS field experiment, Atmos. Chem. Phys., 14, 8449–8460, https://doi.org/10.5194/acp-14-8449-2014, 2014.

Garofalo, L. A., Pothier, M. A., Levin, E. J. T., Campos, T., Kreidenweis, S. M., and Farmer, D. K.: Emission and Evolution of Submicron Organic Aerosol in Smoke from Wildfires in the Western United States, ACS Earth Space Chem., 3, 1237–1247, https://doi.org/10.1021/acsearthspacechem.9b00125, 2019.

Gratz, L. E., Jaffe, D. A., and Hee, J. R.: Causes of increasing ozone and decreasing carbon monoxide in springtime at the Mt. Bachelor Observatory from 2004 to 2013, Atmos. Environ., 109, 323–330, https://doi.org/10.1016/j.atmosenv.2014.05.076, 2015.

Grimm, H. and Eatough, D.: Aerosol Measurement: The Use of Optical Light Scattering for the Determination of Particulate Size Distribution, and Particulate Mass, Including the Semi-Volatile Fraction, J. Air Waste Manage. Assoc., 59, 101–107, https://doi.org/10.3155/1047-3289.59.1.101, 2009.

Hand, J. L. and Malm, W. C.: Review of aerosol mass scattering efficiencies from ground-based measurements since 1990, J. Geophys. Res., 112, D16203, https://doi.org/10.1029/2007JD008484, 2007.

Healy, R. M., Wang, J. M., Jeong, C.-H., Lee, A. K. Y., Willis, M. D., Jaroudi, E., Zimmerman, N., Hilker, N., Murphy, M., Eckhardt, S., Stohl, A., Abbatt, J. P. D., Wenger, J. C., and Evans, G. J.: Light-absorbing properties of ambient black carbon and brown carbon from fossil fuel and biomass burning sources, J. Geophys. Res.-Atmos., 120, 6619–6633, https://doi.org/10.1002/2015JD023382, 2015.

Hems, R. F., Schnitzler, E. G., Liu-Kang, C., Cappa, C. D., and Abbatt, J. P. D.: Aging of Atmospheric Brown Carbon Aerosol, ACS Earth Space Chem., 5, 722–748, https://doi.org/10.1021/acsearthspacechem.0c00346, 2021.

Hobbs, P. v., Sinha, P., Yokelson, R. J., Christian, T. J., Blake, D. R., Gao, S., Kirchstetter, T. W., Novakov, T., and Pilewskie, P.: Evolution of gases and particles from a savanna fire in South Africa, J. Geophys. Res.-Atmos., 108, 8485, https://doi.org/10.1029/2002jd002352, 2003.

Hodshire, A. L., Akherati, A., Alvarado, M. J., Brown-Steiner, B., Jathar, S. H., Jimenez, J. L., Kreidenweis, S. M., Lonsdale, C. R., Onasch, T. B., Ortega, A. M., and Pierce, J. R.: Aging Effects on Biomass Burning Aerosol Mass and Composition: A Critical Review of Field and Laboratory Studies, Environ. Sci. Technol., 53, 10007–10022, https://doi.org/10.1021/acs.est.9b02588, 2019.

Hosseini, S., Li, Q., Cocker, D., Weise, D., Miller, A., Shrivastava, M., Miller, J. W., Mahalingam, S., Princevac, M., and Jung, H.: Particle size distributions from laboratory-scale biomass fires using fast response instruments, Atmos.Chem. Phys., 10, 8065–8076, https://doi.org/10.5194/acp-10-8065-2010, 2010.

Jaffe, D.: Mt. Bachelor Observatory final atmospheric data (v1) for Year 2019, University of Washington's Research Works Archive [data set], http://hdl.handle.net/1773/48342, last access: 23 February 2023.

Jaffe, D. A., O'Neill, S. M., Larkin, N. K., Holder, A. L., Peterson, D. L., Halofsky, J. E., and Rappold, A. G.: Wildfire and prescribed burning impacts on air quality in the United States, J. Air Waste Manage. Assoc., 70, 583–615, https://doi.org/10.1080/10962247.2020.1749731, 2020.

Jahn, L. G., Jahl, L. G., Bland, G. D., Bowers, B. B., Monroe, L. W., and Sullivan, R. C.: Metallic and Crustal Elements in Biomass-Burning Aerosol and Ash: Prevalence, Significance, and Similarity to Soil Particles, ACS Earth Space Chem., 5, 136–148, https://doi.org/10.1021/acsearthspacechem.0c00191, 2021.

Johnson, M. S., Strawbridge, K., Knowland, K. E., Keller, C., and Travis, M.: Long-range transport of Siberian biomass burning emissions to North America during FIREX-AQ, Atmos. Environ., 252, 118241, https://doi.org/10.1016/j.atmosenv.2021.118241, 2021.

Jolleys, M. D., Coe, H., McFiggans, G., Taylor, J. W., O'Shea, S. J., le Breton, M., Bauguitte, S. J.-B., Moller, S., di Carlo, P., Aruffo, E., Palmer, P. I., Lee, J. D., Percival, C. J., and Gallagher, M. W.: Properties and evolution of biomass burning organic aerosol from Canadian boreal forest fires, Atmos. Chem. Phys., 15, 3077–3095, https://doi.org/10.5194/acp-15-3077-2015, 2015.

Jung, C. H., Lee, J. Y., and Kim, Y. P.: Changes in the ångstrom exponent during aerosol coagulation and condensation, Asian J. Atmos. Environ., 6, 304–313, https://doi.org/10.5572/ajae.2012.6.4.304, 2012.

Kaaden, N., Massling, A., Schladitz, A., MüLLER, T., Kandler, K., Schütz, L., Weinzierl, B., Petzold, A., Tesche, M., Leinert, S., Deutscher, C., Ebert, M., Weinbruch, S., and Wiedensohler, A.: State of mixing, shape factor, number size distribution, and hygroscopic growth of the Saharan anthropogenic and mineral dust aerosol at Tinfou, Morocco, Tellus B, 61, 51–63, https://doi.org/10.1111/j.1600-0889.2008.00388.x, 2009.

Kandler, K., Schütz, L., Deutscher, C., Ebert, M., Hofmann, H., Jäckel, S., Jaenicke, R., Knippertz, P., Lieke, K., Massling, A., Petzold, A., Schladitz, A., Weinzierl, B., Wiedensohler, A., Zorn, S., and Weinbruch1, S.: Size distribution, mass concentration, chemical and mineralogical composition and derived optical parameters of the boundary layer aerosol at Tinfou, Morocco, during SAMUM 2006, Tellus B, 61, 32–50, https://doi.org/10.1111/j.1600-0889.2008.00385.x, 2009.

Kirchstetter, T. W. and Thatcher, T. L.: Contribution of organic carbon to wood smoke particulate matter absorption of solar radiation, Atmos. Chem. Phys., 12, 6067–6072, https://doi.org/10.5194/acp-12-6067-2012, 2012.

Kleinman, L. I., Sedlacek III, A. J., Adachi, K., Buseck, P. R., Collier, S., Dubey, M. K., Hodshire, A. L., Lewis, E., Onasch, T. B., Pierce, J. R., Shilling, J., Springston, S. R., Wang, J., Zhang, Q., Zhou, S., and Yokelson, R. J.: Rapid evolution of aerosol particles and their optical properties downwind of wildfires in the western US, Atmos. Chem. Phys., 20, 13319–13341, https://doi.org/10.5194/acp-20-13319-2020, 2020.

Kondo, Y., Matsui, H., Moteki, N., Sahu, L., Takegawa, N., Kajino, M., Zhao, Y., Cubison, M. J., Jimenez, J. L., Vay, S., Diskin, G. S., Anderson, B., Wisthaler, A., Mikoviny, T., Fuelberg, H. E., Blake, D. R., Huey, G., Weinheimer, A. J., Knapp, D. J., and Brune, W. H.: Emissions of black carbon, organic, and inorganic aerosols from biomass burning in North America and Asia in 2008, J. Geophys. Res., 116, D08204, https://doi.org/10.1029/2010JD015152, 2011.

Konovalov, I. B., Golovushkin, N. A., Beekmann, M., and Andreae, M. O.: Insights into the aging of biomass burning aerosol from satellite observations and 3D atmospheric modeling: evolution of the aerosol optical properties in Siberian wildfire plumes, Atmos. Chem. Phys., 21, 357–392, https://doi.org/10.5194/acp-21-357-2021, 2021.

Lack, D. A. and Langridge, J. M.: On the attribution of black and brown carbon light absorption using the Ångström exponent, Atmos. Chem. Phys., 13, 10535–10543, https://doi.org/10.5194/acp-13-10535-2013, 2013.

Laing, J. R., Jaffe, D. A., and Hee, J. R.: Physical and optical properties of aged biomass burning aerosol from wildfires in Siberia and the Western USA at the Mt. Bachelor Observatory, Atmos. Chem. Phys., 16, 15185–15197, https://doi.org/10.5194/acp-16-15185-2016, 2016.

Laing, J. R., Jaffe, D. A., and Sedlacek Arthur J., I. I. I.: Comparison of Filter-based Absorption Measurements of Biomass Burning Aerosol and Background Aerosol at the Mt. Bachelor Observatory, Aerosol Air Qual. Res., 20, 663–678, https://doi.org/10.4209/aaqr.2019.06.0298, 2020.

Laskin, A., Laskin, J., and Nizkorodov, S. A.: Chemistry of Atmospheric Brown Carbon, Chem. Rev., 115, 4335–4382, https://doi.org/10.1021/cr5006167, 2015.

Lee, Y.-G. and Cho, C.-H.: Characteristics of Aerosol Size Distribution for a Severe Asian Dust Event Observed at Anmyeon, Korea in April 2006, J. Korean Meteorol. Soc., 43, 87–96, 2007.

Levin, E. J. T., McMeeking, G. R., Carrico, C. M., Mack, L. E., Kreidenweis, S. M., Wold, C. E., Moosmüller, H., Arnott, W. P., Hao, W. M., Collett, J. L., and Malm, W. C.: Biomass burning smoke aerosol properties measured during Fire Laboratory at Missoula Experiments (FLAME), J. Geophys. Res., 115, D18210, https://doi.org/10.1029/2009JD013601, 2010.

Li, C., He, Q., Hettiyadura, A. P. S., Käfer, U., Shmul, G., Meidan, D., Zimmermann, R., Brown, S. S., George, C., Laskin, A., and Rudich, Y.: Formation of Secondary Brown Carbon in Biomass Burning Aerosol Proxies through NO_3 Radical Reactions, Environ. Sci. Technol., 54, 1395–1405, https://doi.org/10.1021/acs.est.9b05641, 2020.

Li, M., Shen, F., and Sun, X.: 2019–2020 Australian bushfire air particulate pollution and impact on the South Pacific Ocean, Sci. Rep., 11, 12288, https://doi.org/10.1038/s41598-021-91547-y, 2021.

Liang, C.-S., Yu, T.-Y., Chang, Y.-Y., Syu, J.-Y., and Lin, W.-Y.: Source Apportionment of $PM_{2.5}$ Particle Composition and Submicrometer Size Distribution during an Asian Dust Storm and Non-Dust Storm in Taipei, Aerosol Air Qual. Res., 13, 545–554, https://doi.org/10.4209/aaqr.2012.06.0161, 2013.

Liao, J., Wolfe, G. M., Hannun, R. A., st. Clair, J. M., Hanisco, T. F., Gilman, J. B., Lamplugh, A., Selimovic, V., Diskin, G. S., Nowak, J. B., Halliday, H. S., DiGangi, J. P., Hall, S. R., Ullmann, K., Holmes, C. D., Fite, C. H., Agastra, A., Ryerson, T. B., Peischl, J., Bourgeois, I., Warneke, C., Coggon, M. M., Gkatzelis, G. I., Sekimoto, K., Fried, A., Richter, D., Weibring, P., Apel, E. C., Hornbrook, R. S., Brown, S. S., Womack, C. C., Robinson, M. A., Washenfelder, R. A., Veres, P.

R., and Neuman, J. A.: Formaldehyde evolution in US wildfire plumes during the Fire Influence on Regional to Global Environments and Air Quality experiment (FIREX-AQ), Atmos. Chem. Phys., 21, 18319–18331, https://doi.org/10.5194/acp-21-18319-2021, 2021.

Liu, D., He, C., Schwarz, J. P., and Wang, X.: Lifecycle of light-absorbing carbonaceous aerosols in the atmosphere, npj Clim. Atmos. Sci., 3, 40, https://doi.org/10.1038/s41612-020-00145-8, 2020a.

Liu, D., Hu, K., Zhao, D., Ding, S., Wu, Y., Zhou, C., Yu, C., Tian, P., Liu, Q., Bi, K., Wu, Y., Hu, B., Ji, D., Kong, S., Ouyang, B., He, H., Huang, M., and Ding, D.: Efficient Vertical Transport of Black Carbon in the Planetary Boundary Layer, Geophys. Res. Lett., 47, e2020GL088858, https://doi.org/10.1029/2020GL088858, 2020b.

Liu, D., Li, S., Hu, D., Kong, S., Cheng, Y., Wu, Y., Ding, S., Hu, K., Zheng, S., Yan, Q., Zheng, H., Zhao, D., Tian, P., Ye, J., Huang, M., and Ding, D.: Evolution of Aerosol Optical Properties from Wood Smoke in Real Atmosphere Influenced by Burning Phase and Solar Radiation, Environ. Sci. Technol., 55, 5677–5688, https://doi.org/10.1021/acs.est.0c07569, 2021.

Liu, Y., Goodrick, S., and Heilman, W.: Wildland fire emissions, carbon, and climate: Wildfire–climate interactions, Forest Ecol. Manage., 317, 80–96, https://doi.org/10.1016/j.foreco.2013.02.020, 2014.

Lowenthal, D. H. and Kumar, N.: Variation of mass scattering efficiencies in IMPROVE, J. Air Waste Manage. Assoc., 54, 926–934, https://doi.org/10.1080/10473289.2004.10470969, 2004.

Makar, P. A., Akingunola, A., Chen, J., Pabla, B., Gong, W., Stroud, C., Sioris, C., Anderson, K., Cheung, P., Zhang, J., and Milbrandt, J.: Forest-fire aerosol–weather feedbacks over western North America using a high-resolution, online coupled air-quality model, Atmos. Chem. Phys., 21, 10557–10587, https://doi.org/10.5194/acp-21-10557-2021, 2021.

Maudlin, L. C., Wang, Z., Jonsson, H. H., and Sorooshian, A.: Impact of wildfires on size-resolved aerosol composition at a coastal California site, Atmos. Environ., 119, 59–68, https://doi.org/10.1016/j.atmosenv.2015.08.039, 2015.

May, A. A., Levin, E. J. T., Hennigan, C. J., Riipinen, I., Lee, T., Collett, J. L., Jimenez, J. L., Kreidenweis, S. M., and Robinson, A. L.: Gas-particle partitioning of primary organic aerosol emissions: 3. Biomass burning, J. Geophys. Res.-Atmos., 118, 11327–11338, https://doi.org/10.1002/jgrd.50828, 2013.

May, A. A., McMeeking, G. R., Lee, T., Taylor, J. W., Craven, J. S., Burling, I., Sullivan, A. P., Akagi, S., Collett, J. L., Flynn, M., Coe, H., Urbanski, S. P., Seinfeld, J. H., Yokelson, R. J., and Kreidenweis, S. M.: Aerosol emissions from prescribed fires in the United States: A synthesis of laboratory and aircraft measurements, J. Geophys. Res.-Atmos., 119, 11826–11849, https://doi.org/10.1002/2014JD021848, 2014.

McMeeking, G. R.: Observations of smoke-influenced aerosol during the Yosemite Aerosol Characterization Study: Size distributions and chemical composition, J. Geophys. Res., 110, D09206, https://doi.org/10.1029/2004JD005389, 2005.

Mohr, C., Lopez-Hilfiker, F. D., Zotter, P., Prévôt, A. S. H., Xu, L., Ng, N. L., Herndon, S. C., Williams, L. R., Franklin, J. P., Zahniser, M. S., Worsnop, D. R., Knighton, W. B., Aiken, A. C., Gorkowski, K. J., Dubey, M. K., Allan, J. D., and Thornton, J. A.: Contribution of Nitrated Phenols to Wood Burning Brown Carbon Light Absorption in Detling, United Kingdom during Winter Time, Environ. Sci. Technol., 47, 6316–6324, https://doi.org/10.1021/es400683v, 2013.

Mori, T., Kondo, Y., Ohata, S., Zhao, Y., Sinha, P. R., Oshima, N., Matsui, H., Moteki, N., and Koike, M.: Seasonal Variation of Wet Deposition of Black Carbon in Arctic Alaska, J. Geophys. Res.-Atmos., 125, e2019JD032240, https://doi.org/10.1029/2019JD032240, 2020.

Nguyen, T. B., Laskin, A., Laskin, J., and Nizkorodov, S. A.: Brown carbon formation from ketoaldehydes of biogenic monoterpenes, Faraday Discuss., 165, 473–494, https://doi.org/10.1039/C3FD00036B, 2013.

Nisantzi, A., Mamouri, R. E., Ansmann, A., and Hadjimitsis, D.: Injection of mineral dust into the free troposphere during fire events observed with polarization lidar at Limassol, Cyprus, Atmos. Chem. Phys., 14, 12155–12165, https://doi.org/10.5194/acp-14-12155-2014, 2014.

Pierce, J. R., Chen, K., and Adams, P. J.: Contribution of primary carbonaceous aerosol to cloud condensation nuclei: processes and uncertainties evaluated with a global aerosol microphysics model, Atmos. Chem. Phys., 7, 5447–5466, https://doi.org/10.5194/acp-7-5447-2007, 2007.

Popovicheva, O., Kistler, M., Kireeva, E., Persiantseva, N., Timofeev, M., Kopeikin, V., and Kasper-Giebl, A.: Physicochemical characterization of smoke aerosol during large-scale wildfires: Extreme event of August 2010 in Moscow, Atmos. Environ., 96, 405–414, https://doi.org/10.1016/j.atmosenv.2014.03.026, 2014.

Raut, J.-C., Marelle, L., Fast, J. D., Thomas, J. L., Weinzierl, B., Law, K. S., Berg, L. K., Roiger, A., Easter, R. C., Heimerl, K., Onishi, T., Delanoë, J., and Schlager, H.: Cross-polar transport and scavenging of Siberian aerosols containing black carbon during the 2012 ACCESS summer campaign, Atmos. Chem. Phys., 17, 10969–10995, https://doi.org/10.5194/acp-17-10969-2017, 2017.

Reid, J. S., Koppmann, R., Eck, T. F., and Eleuterio, D. P.: A review of biomass burning emissions part II: intensive physical properties of biomass burning particles, Atmos. Chem. Phys., 5, 799–825, https://doi.org/10.5194/acp-5-799-2005, 2005.

Russell, P. B., Redemann, J., Schmid, B., Bergstrom, R. W., Livingston, J. M., McIntosh, D. H., Ramirez, S. A., Hartley, S., Hobbs, P. V., Quinn, P. K., Carrico, C. M., Rood, M. J., Ostrom, E., Noone, K. J., von Hoyningen-Huene, W., and Remer, L.: Comparison of aerosol single-scattering albedos derived by diverse techniques in two North Atlantic experiments, J. Atmos Sci., 59, 609–619, 2002.

Saleh, R.: From Measurements to Models: Toward Accurate Representation of Brown Carbon in Climate Calculations, Curr. Poll. Rep., 6, 90–104, 2020.

Schlosser, J. S., Braun, R. A., Bradley, T., Dadashazar, H., MacDonald, A. B., Aldhaif, A. A., Aghdam, M. A., Mardi, A. H., Xian, P., and Sorooshian, A.: Analysis of aerosol composition data for western United States wildfires between 2005 and 2015: Dust emissions, chloride depletion, and most enhanced aerosol constituents, J. Geophys. Res.-Atmos., 122, 8951–8966, https://doi.org/10.1002/2017JD026547, 2017.

Seinfeld, J. H. and Pandis, S. N.: Atmospheric chemistry and physics: From air pollution to climate change, https://heronet.epa.gov/heronet/index.cfm/reference/download/reference_id/2079502 (last access: 23 February 2023), 2006.

Spracklen, D. v., Carslaw, K. S., Pöschl, U., Rap, A., and Forster, P. M.: Global cloud condensation nuclei influenced by carbonaceous combustion aerosol, Atmos. Chem. Phys., 11, 9067–9087, https://doi.org/10.5194/acp-11-9067-2011, 2011.

Stocks, B. J., Fosberg, M. A., Lynham, T. J., Mearns, L., Wotton, B. M., Yang, Q., Jin, J.-Z., Lawrence, K., Hartley, G. R., Mason, J. A., and McKenney, D. W.: Climate Change and Forest Fire Potential in Russian and Canadian Boreal Forests, Climatic Change, 38, 1–13, https://doi.org/10.1023/A:1005306001055, 1998.

Taylor, J. W., Allan, J. D., Allen, G., Coe, H., Williams, P. I., Flynn, M. J., le Breton, M., Muller, J. B. A., Percival, C. J., Oram, D., Forster, G., Lee, J. D., Rickard, A. R., Parrington, M., and Palmer, P. I.: Size-dependent wet removal of black carbon in Canadian biomass burning plumes, Atmos. Chem. Phys., 14, 13755–13771, https://doi.org/10.5194/acp-14-13755-2014, 2014.

Titos, G., Ealo, M., Pandolfi, M., Pérez, N., Sola, Y., Sicard, M., Comerón, A., Querol, X., and Alastuey, A.: Spatiotemporal evolution of a severe winter dust event in the western Mediterranean: Aerosol optical and physical properties, J. Geophys. Res.-Atmos., 122, 4052–4069, https://doi.org/10.1002/2016JD026252, 2017.

Tröstl, J., Herrmann, E., Frege, C., Bianchi, F., Molteni, U., Bukowiecki, N., Hoyle, C. R., Steinbacher, M., Weingartner, E., Dommen, J., Gysel, M., and Baltensperger, U.: Contribution of new particle formation to the total aerosol concentration at the high-altitude site Jungfraujoch (3580 m asl, Switzerland), J. Geophys. Res.-Atmos., 121, 11692–11711, https://doi.org/10.1002/2015JD024637, 2016.

Updyke, K. M., Nguyen, T. B., and Nizkorodov, S. A.: Formation of brown carbon via reactions of ammonia with secondary organic aerosols from biogenic and anthropogenic precursors, Atmos. Environ., 63, 22–31, https://doi.org/10.1016/j.atmosenv.2012.09.012, 2012.

Vakkari, V., Kerminen, V., Beukes, J. P., Tiitta, P., Zyl, P. G., Josipovic, M., Venter, A. D., Jaars, K., Worsnop, D. R., Kulmala, M., and Laakso, L.: Rapid changes in biomass burning aerosols by atmospheric oxidation, Geophys. Res. Lett., 41, 2644–2651, https://doi.org/10.1002/2014GL059396, 2014.

Virkkula, A.: Correction of the Calibration of the 3-wavelength Particle Soot Absorption Photometer (3λ PSAP), Aerosol Sci. Tech., 44, 706–712, https://doi.org/10.1080/02786826.2010.482110, 2010.

Virkkula, A., Ahlquist, N. C., Covert, D. S. Arnott, W. P. Sheridan, P. J., Quinn, P. K., and Coffman, D. J.: Modification, Calibration and a Field Test of an Instrument for Measuring Light Absorption by Particles, Aerosol Sci. Tech., 39, 68–83, 2005.

Wagner, R., Jähn, M., and Schepanski, K.: Wildfires as a source of airborne mineral dust – revisiting a conceptual model using large-eddy simulation (LES), Atmos. Chem. Phys., 18, 11863–11884, https://doi.org/10.5194/acp-18-11863-2018, 2018.

Weiss-Penzias, P., Jaffe, D. A., Swartzendruber, P., Dennison, J. B., Chand, D., Hafner, W., and Prestbo, E.: Observations of Asian air pollution in the free troposphere at Mount Bachelor Observatory during the spring of 2004, J. Geophys. Res.-Atmos., 111, D10304, https://doi.org/10.1029/2005JD006522, 2006.

Westerling, A. L.: Increasing western US forest wildfire activity: sensitivity to changes in the timing of spring, Philos. T. Roy. Soc. B, 371, 20150178, https://doi.org/10.1098/rstb.2015.0178, 2016.

Wigder, N. L., Jaffe, D. A., and Saketa, F. A.: Ozone and particulate matter enhancements from regional wildfires observed at Mount Bachelor during 2004–2011, Atmos. Environ., 75, 24–31, https://doi.org/10.1016/j.atmosenv.2013.04.026, 2013.

Wiggins, E. B., Anderson, B. E., Brown, M. D., Campuzano-Jost, P., Chen, G., Crawford, J., Crosbie, E. C., Dibb, J., DiGangi, J. P., Diskin, G. S., Fenn, M., Gallo, F., Gargulinski, E. M., Guo, H., Hair, J. W., Halliday, H. S., Ichoku, C., Jimenez, J. L., Jordan, C. E., Katich, J. M., Nowak, J. B., Perring, A. E., Robinson, C. E., Sanchez, K. J., Schueneman, M., Schwarz, J. P., Shingler, T. J., Shook, M. A., Soja, A. J., Stockwell, C. E., Thornhill, K. L., Travis, K. R., Warneke, C., Winstead, E. L., Ziemba, L. D., and Moore, R. H.: Reconciling Assumptions in Bottom-Up and Top-Down Approaches for Estimating Aerosol Emission Rates From Wildland Fires Using Observations From FIREX-AQ, J. Geophys. Res.-Atmos., 126, e2021JD035692, https://doi.org/10.1029/2021JD035692, 2021.

Winker, D. M., Pelon, J., Coakley, J. A., Ackerman, S. A., Charlson, R. J., Colarco, P. R., Flamant, P., Fu, Q., Hoff, R. M., Kittaka, C., Kubar, T. L., le Treut, H., Mccormick, M. P., Mégie, G., Poole, L., Powell, K., Trepte, C., Vaughan, M. A., and Wielicki, B. A.: The CALIPSO Mission, B. Am. Meteorol. Soc., 91, 1211–1230, https://doi.org/10.1175/2010BAMS3009.1, 2010.

Wu, H., Taylor, J. W., Langridge, J. M., Yu, C., Allan, J. D., Szpek, K., Cotterell, M. I., Williams, P. I., Flynn, M., Barker, P., Fox, C., Allen, G., Lee, J., and Coe, H.: Rapid transformation of ambient absorbing aerosols from West African biomass burning, Atmos. Chem. Phys., 21, 9417–9440, https://doi.org/10.5194/acp-21-9417-2021, 2021.

Xu, L., Crounse, J. D., Vasquez, K. T., Allen, H., Wennberg, P. O., Bourgeois, I., Brown, S. S., Campuzano-Jost, P., Coggon, M. M., Crawford, J. H., DiGangi, J. P., Diskin, G. S., Fried, A., Gargulinski, E. M., Gilman, J. B., Gkatzelis, G. I., Guo, H., Hair, J. W., Hall, S. R., Halliday, H. A., Hanisco, T. F., Hannun, R. A., Holmes, C. D., Huey, L. G., Jimenez, J. L., Lamplugh, A., Lee, Y. R., Liao, J., Lindaas, J., Neuman, J. A., Nowak, J. B., Peischl, J., Peterson, D. A., Piel, F., Richter, D., Rickly, P. S., Robinson, M. A., Rollins, A. W., Ryerson, T. B., Sekimoto, K., Selimovic, V., Shingler, T., Soja, A. J., st. Clair, J. M., Tanner, D. J., Ullmann, K., Veres, P. R., Walega, J., Warneke, C., Washenfelder, R. A., Weibring, P., Wisthaler, A., Wolfe, G. M., Womack, C. C., and Yokelson, R. J.: Ozone chemistry in western U.S. wildfire plumes, Sci. Adv., 7, eabl3648, https://doi.org/10.1126/sciadv.abl3648, 2021.

Yokelson, R. J., Crounse, J. D., DeCarlo, P. F., Karl, T., Urbanski, S., Atlas, E., Campos, T., Shinozuka, Y., Kapustin, V., Clarke, A. D., Weinheimer, A., Knapp, D. J., Montzka, D. D., Holloway, J., Weibring, P., Flocke, F., Zheng, W., Toohey, D., Wennberg, P. O., Wiedinmyer, C., Mauldin, L., Fried, A., Richter, D., Walega, J., Jimenez, J. L., Adachi, K., Buseck, P. R., Hall, S. R., and Shetter, R.: Emissions from biomass burning in the Yucatan, Atmos. Chem. Phys., 9, 5785–5812, https://doi.org/10.5194/acp-9-5785-2009, 2009.

Zhang, L. and Jaffe, D. A.: Trends and sources of ozone and sub-micron aerosols at the Mt. Bachelor Observatory (MBO) during 2004–2015, Atmos. Environ., 165, 143–154, https://doi.org/10.1016/j.atmosenv.2017.06.042, 2017.

Zhang, X., Mao, M., Chen, H., and Tang, S.: Theoretical study of scattering Angstrom exponent of coated black carbon aerosols: The effect of microphysical configurations, J. Quant. Spectrosc. Ra., 256, 107302, https://doi.org/10.1016/j.jqsrt.2020.107302, 2020.

Zhou, S., Collier, S., Jaffe, D. A., Briggs, N. L., Hee, J., Iii, A. J. S., Kleinman, L., Onasch, T. B., and Zhang, Q.: Regional influence of wildfires on aerosol chemistry in the western US and insights into atmospheric aging of biomass burning organic aerosol, Atmos. Chem. Phys., 17, 2477–2493, https://doi.org/10.5194/acp-17-2477-2017, 2017.

Zhou, S., Collier, S., Jaffe, D. A., and Zhang, Q.: Free tropospheric aerosols at the Mt. Bachelor Observatory: more oxidized and higher sulfate content compared to boundary layer aerosols, Atmos. Chem. Phys., 19, 1571–1585, https://doi.org/10.5194/acp-19-1571-2019, 2019.